

A mechanistic model for the spectral induced polarization of clay materials

Philippe Leroy, André Revil

▶ **To cite this version:**

Philippe Leroy, André Revil. A mechanistic model for the spectral induced polarization of clay materials. Journal of Geophysical Research : Solid Earth, 2009, 114, pp.B10202. 10.1029/2008JB006114 . insu-00498792

HAL Id: insu-00498792
https://insu.hal.science/insu-00498792

Submitted on 8 Mar 2021

HAL is a multi-disciplinary open access archive for the deposit and dissemination of scientific research documents, whether they are published or not. The documents may come from teaching and research institutions in France or abroad, or from public or private research centers.

L'archive ouverte pluridisciplinaire **HAL**, est destinée au dépôt et à la diffusion de documents scientifiques de niveau recherche, publiés ou non, émanant des établissements d'enseignement et de recherche français ou étrangers, des laboratoires publics ou privés.

A mechanistic model for the spectral induced polarization of clay materials

P. Leroy[1] and A. Revil[2,3]

Received 25 September 2008; revised 31 May 2009; accepted 9 July 2009; published 6 October 2009.

[1] Water-saturated clay-rich media exhibit low-frequency (1 Hz to 1 MHz) effective conductivity and effective permittivity dispersions that are the consequence of both the polarization of the mineral/water interface coating the surface of the grains and the Maxwell-Wagner polarization. These low-frequency properties are modeled by combining (1) a complexation model of the surface properties of clay minerals (kaolinite, illite, and smectite), (2) a polarization model of the Stern layer (the inner portion of the electrical double layer coating the surface of the minerals), and (3) a macroscopic model comprising the electrochemical polarization of the grains and the contribution of the Maxwell-Wagner effect. The macroscopic model is based on the differential effective medium theory. It includes a convolution product with the grain size distribution. For kaolinite, the diffuse layer occupies a small fraction of the pore space and is considered as part of the surface of the grains. This is due to the low specific surface area of kaolinite. In the case of illite and smectite, the situation is different. Because of the high specific surface areas of these minerals, the diffuse layer occupies a large fraction of the pore space and is considered as part of the pore space and is described using a Donnan equilibrium model. We obtain excellent comparisons between various experimental data reported in the literature and our model. Then, we considered low-porosity (compacted or cemented) clay rocks and shales. Here too, we obtained a good agreement between the data and the predictions of a model based on a volume-averaging approach. We also note that at very low frequencies (<1 Hz), another polarization mechanism exists that is not reproduced by our model. We believe that this polarization corresponds to a nonlinear membrane polarization contribution.

Citation: Leroy, P., and A. Revil (2009), A mechanistic model for the spectral induced polarization of clay materials, *J. Geophys. Res.*, *114*, B10202, doi:10.1029/2008JB006114.

1. Introduction

[2] If a constant current is injected though a water-saturated porous rock or in the ground and shut down, the voltage measured between two electrodes decays more or less slowly over time. This phenomenon is investigated by a geophysical method called time domain induced polarization. Spectral induced polarization (SIP) (also called complex conductivity, complex resistivity, or dielectric spectroscopy) reports the magnitude and the phase between the electrical current and the voltage for various frequencies generally between few kHz or few MHz. In both cases, induced polarization is associated with the storage of electrical charges that accompany the electromigration of charge carriers (electrons and ions) in porous materials and electrochemical activity at interfaces between various phases. Various mechanisms of charge storage have been discussed in the literature including oxidoreduction phenomena, cation exchange capacity, and Maxwell-Wagner polarization, just to cite few of them (see *Olhoeft* [1985] for an early review).

[3] Historically, induced polarization has been developed to locate mineral deposits like massive or pervasive ore bodies [*Zhdanov and Keller*, 1994]. In the case of ore bodies, induced polarization is generated by the accumulation of ions at the surface of electronic conductors [*Mansoor and Slater*, 2007, and references therein]. There is also a rich literature in the application of induced polarization in oil fields as a downhole measurement method [e.g., *Vinegar and Waxman*, 1982, 1984, 1987]. *Park and Dickey* [1989] used Vinegar and Waxman's work for one of the early published hydrogeophysical studies using this method.

[4] Recently, the SIP method has been the focus of a high number of research works in environmental geophysics for two main reasons: (1) induced polarization spectra bear information that can be useful to determine the hydraulic conductivity of rocks [*Arulanandan*, 1969; *Börner and Schön*, 1991; *Weller and Börner*, 1996; *Slater and Lesmes*, 2002; *Scott and Barker*, 2003; *Kemna et al.*, 2004; *Hördt et*

[1]BRGM, Orléans, France.
[2]Department of Geophysics, Colorado School of Mines, Golden, Colorado, USA.
[3]Laboratoire de Géophysique Interne et Tectophysique, Campus Scientifique, Université de Savoie, CNRS, Le-Bourget-du-Lac, France.

Copyright 2009 by the American Geophysical Union.
0148-0227/09/2008JB006114$09.00

al., 2007; *Ghorbani et al.*, 2007; *Slater*, 2007; *Tarasov and Titov*, 2007] and (2) induced polarization is sensitive to the sorption of organic and inorganic contaminants and can be therefore used to delineate contaminant plumes [*Börner et al.*, 1993; *Grimm et al.*, 2005; *Sogade et al.*, 2006; *Radic*, 2007].

[5] Because clay minerals are abundant in nature and they are known to have a strong impact on the hydraulic and electrical properties of rocks [*Arulanandan*, 1969; *Alali*, 2007; *Santiwong et al.*, 2008], it is important to understand their low-frequency SIP responses [*Korosak et al.*, 2007; *Samec et al.*, 2007]. In contaminated areas, back diffusion of some contaminants from clayey materials needs also to be better assessed/imaged using geophysical methods for remediation purposes. Induced polarization is likely to be a suitable tool for such a problem.

[6] A number of experimental works [e.g., *Schwan et al.*, 1962; *Ballario et al.*, 1976; *Poley et al.*, 1978; *Lockhart*, 1980; *Olhoeft*, 1979, 1985; *Korosak et al.*, 2007] have shown that the low-frequency complex conductivity and permittivity responses of water-saturated porous materials exhibit dispersion phenomena in the frequency range 1 mHz to 1 MHz. *Cole and Cole* [1941], *Davidson and Cole* [1951], *Jonscher* [1983], and *Wait* [1984] proposed phenomenological models fitting the complex conductivity (permittivity) data at low frequencies. However, these models are not very useful if we cannot connect a mechanistic model of polarization to the macroscopic parameters used to fit the data (e.g., the Cole-Cole parameters [see *Ghorbani et al.*, 2007]). They teach us nothing, for example, about the potential effects of contaminant upon induced polarization spectra.

[7] As said above, there are several mechanisms of charge storage in porous media. One of them is the polarization of the grains. Mechanistic models corresponding to this contribution have been proposed by *Schwarz* [1962], *Dukhin and Shilov* [1974], and *Fixman* [1980]. In thermodynamic equilibrium, a fixed charge density occurs at the surface of all minerals in contact with water because of the chemical reactivity of surface sites like hydroxyl groups (e.g., silanol or aluminol groups). This fixed charge density is partly counterbalanced in a layer of sorbed counterions (the Stern layer). Additional counterions and coions are located in the so-called electrical diffuse layer extending into the pore space of the porous medium. In the diffuse layer, the ions are linked to the mineral surface through the Coulombic interaction. In an alternating electrical field, the electrical double layer polarizes. The theory of the low-frequency dielectric dispersion has been first elaborated for dilute colloidal suspensions of homogeneous spherical insulating particles surrounded by a thin double layer [*Schwarz*, 1962; *Schurr*, 1964; *Dukhin and Shilov*, 1974; *Fixman*, 1980; *Lyklema et al.*, 1983]. Both the Stern and the diffuse layers become polarized as well as the electrolyte located in the vicinity of the double layer.

[8] The second mechanism of apparent conductivity dispersion is the Maxwell-Wagner dispersion [*Maxwell*, 1892; *Wagner*, 1914]. In a porous composite, the different phases have different conductivities and permittivities. The MW polarization is caused by the formation of field-induced free charge distributions near the interface between the phases of the medium. In the case of granular media like sands, sandstones, and packs of glass beads, models based on the effective medium approximation [e.g., *Bruggeman*, 1935; *Hanai*, 1968; *Sen et al.*, 1981; *Leroy et al.*, 2008] have been successful to model this contribution. Recently, this approach has also been used by *Cosenza et al.* [2008] to model the apparent dielectric spectra of low cation exchange capacity clay rocks showing the strong role of this contribution for such media. In clay rocks, they conclude that electrochemical polarization of the small clay particles can be sometimes hidden by this polarization mechanism. However, we will show in this paper that the Stern layer influences strongly both polarization mechanisms. Indeed, electrochemical polarization in clay media is entirely controlled by the polarization of the Stern layer above 1 Hz. The Stern layer, because of the effect of surface conductivity, is also important to model the Maxwell-Wagner polarization.

[9] *De Lima and Sharma* [1992] and *Endres and Knight* [1992] developed models in which the two contributions discussed above were incorporated into a single petrophysical model. However, these models were not connected explicitly with the electrochemical properties of the mineral/water interface showing explicitly the role of the partition of the counterions between the Stern and the diffuse layers. In addition, the relative importance of the contribution of the polarization of the Stern layer versus the polarization of the diffuse layer was unclear and studied separately in distinct models [see *De Lima and Sharma*, 1992, and references therein]. Recently, *Leroy et al.* [2008] developed a petrophysical model for glass beads in which only the Stern layer polarizes. They argue that the polarization of the diffuse layer can be neglected because the diffuse layer is above a percolation threshold at the scale of a representative elementary volume of rock [*Gonçalvès et al.*, 2007]. *Leroy et al.* [2008] showed that both the Stern and the diffuse layers play a role in the Maxwell-Wagner contribution of SIP because of their anomalous electrical conductivity with respect to the conductivity of the bulk electrolyte. Finally, they use a convolution product to include the particle size distribution in the SIP model [see also *Lesmes and Morgan*, 2001].

[10] In the present paper, we extend the analysis made by *Leroy et al.* [2008] to clays by establishing explicitly the connection between the electrochemical properties of the minerals and their effective conductivity and permittivity spectra at low frequencies. We explicitly show how the availability of the surface sites of the crystalline planes of various clay minerals influence their low-frequency (1 Hz to 1 MHz) electrical behaviors. We also demonstrate that the low-frequency dispersion phenomena are mainly controlled by the polarization of the Stern layer but electrochemical and Maxwell-Wagner polarizations can overlap in the frequency domain. We will show in section 5 that an additional contribution exists below 1 Hz, which may be due to a (nonlinear) membrane polarization mechanism.

2. Electrochemical Properties of Clay Minerals

[11] We provide in this section a triple layer model (TLM) for the different types of clay minerals (essentially kaolinite, illite, and smectite; see Figure 1). A TLM model for kaolinite was developed by *Leroy and Revil* [2004; see

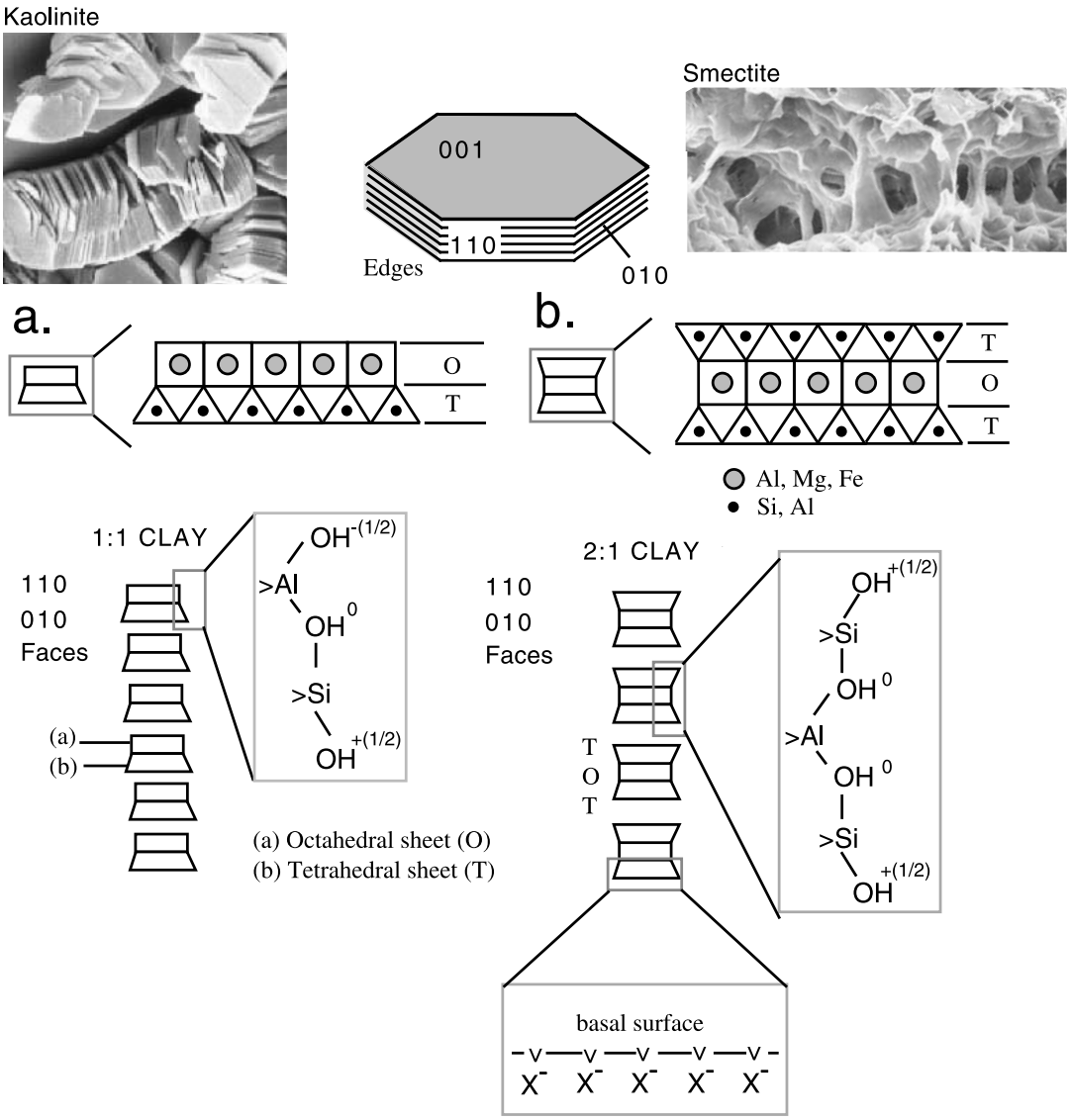


Figure 1. Active surface sites at the edge of (a) 1:1 clays (kaolinite) and (b) 2:1 clays (smectite or illite). In the case of kaolinite, the surface sites are mainly located on the edge of the mineral ({110} and {010} planes). In the case of smectite and illite and in the pH range near neutrality (5 to 9), the surface sites are mainly located on the basal plane ({001} plane) and they are due to isomorphic substitutions inside the crystalline framework (modified from *Leroy and Revil* [2004]). Note also the difference in the morphology of the clay particles. T and O represent tetrahedral and octahedral sheets, respectively.

also *Revil and Leroy*, 2001] and a specific TLM model for the basal crystalline planes of smectite was developed later by *Leroy et al.* [2007]. They are summarized below.

2.1. Complexation of Kaolinite

[12] We consider first a kaolinite crystal in contact with a binary symmetric electrolyte like NaCl (more complex electrolyte can be considered [see *Leroy et al.*, 2007]). We restrict our analysis to the pH range 4–10, which is the pH range useful for most practical applications in geophysics. In this pH range and in the case of kaolinite, the surface mineral reactions at the aluminol, silanol, and > Al–O–Si < surface sites, can be written as [*Leroy and Revil*, 2004]:

$$> \mathrm{AlOH}_2^{1/2+} \Leftrightarrow > \mathrm{AlOH}^{1/2-} + \mathrm{H}^+, K_1, \quad (1)$$

$$> \mathrm{SiOH}^{1/2+} \Leftrightarrow > \mathrm{SiO}^{1/2-} + \mathrm{H}^+, K_2, \quad (2)$$

$$> \mathrm{Al-ONa-Si} < \Leftrightarrow > \mathrm{Al-O^-} - \mathrm{Si} < + \mathrm{Na}^+, K_3, \quad (3)$$

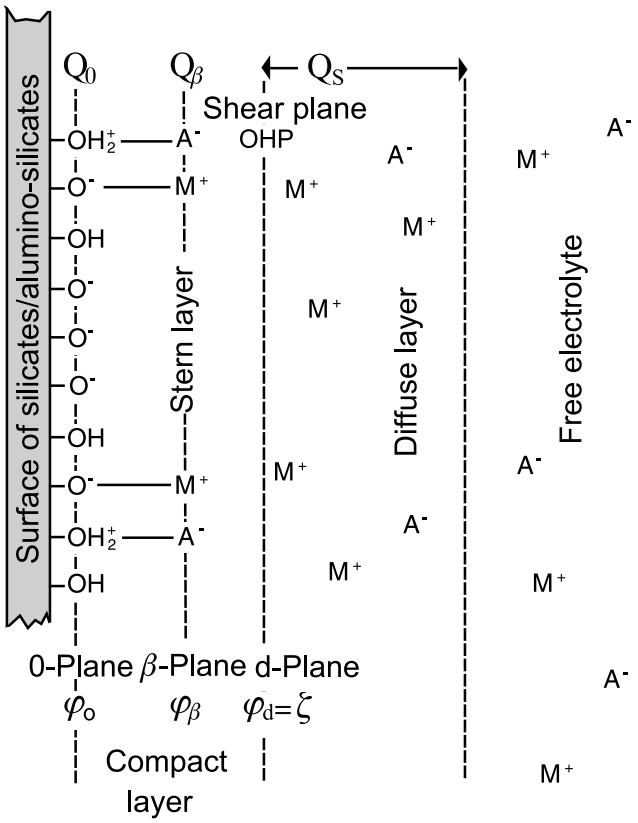


Figure 2. Sketch of the electrical triple-layer model, here for kaolinite (modified from *Leroy and Revil* [2004]). The symbol M represents the metal cations (e.g., Na^+ or K^+) and A represents the anions (e.g., Cl^-). The OHP plane represents the Outer Helmholtz Plane, which coincides here with the shear plane along which the ζ potential arising in electrokinetic phenomena is defined.

where K_1, K_2, and K_3 are the equilibrium constants of reactions (1)–(3), the sign ">" refers to the crystalline framework. The surface site > Al–O–Si < (Figure 1a) carries a net (−1) negative charge [*Avena and De Pauli*, 1996]. We assume that the surface complexation reactions occur on the {010} and {110} planes of kaolinite.

[13] The availability of the surface sites introduced by the chemical reactions described above at the surface of the {010} and {110} planes can be described by the conservation equations for the three types of sites (aluminol, silanol, and > Al–O–Si < surface sites). Solving these equations, we obtain the concentrations of the different surface sites,

$$\Gamma^0_{\mathrm{AlOH}} = \Gamma^0_1/A, \tag{4}$$

$$\Gamma^0_{\mathrm{AlOH_2}} = \frac{\Gamma^0_1}{A}\left(\frac{C^f_{\mathrm{H^+}}}{K_1}\right)\exp\left(-\frac{e\varphi_0}{k_bT}\right), \tag{5}$$

$$\Gamma^0_{\mathrm{SiO}} = \Gamma^0_2/B, \tag{6}$$

$$\Gamma^0_{\mathrm{SiOH}} = \frac{\Gamma^0_2}{B}\left(\frac{C^f_{\mathrm{H^+}}}{K_2}\right)\exp\left(-\frac{e\varphi_0}{k_bT}\right), \tag{7}$$

$$\Gamma^0_{\mathrm{AlOSi}} = \Gamma^0_3/C, \tag{8}$$

$$\Gamma^0_{\mathrm{AlONaSi}} = \frac{\Gamma^0_3}{C}\left(\frac{C^f_{\mathrm{Na^+}}}{K_3}\right)\exp\left(-\frac{e\varphi_\beta}{k_bT}\right), \tag{9}$$

where A, B, and C are given by

$$A = 1 + \frac{C^f_{\mathrm{H^+}}}{K_1}\exp\left(-\frac{e\varphi_0}{k_bT}\right), \tag{10}$$

$$B = 1 + \frac{C^f_{\mathrm{H^+}}}{K_2}\exp\left(-\frac{e\varphi_0}{k_bT}\right), \tag{11}$$

$$C = 1 + \frac{C^f_{\mathrm{Na^+}}}{K_3}\exp\left(-\frac{e\varphi_\beta}{k_bT}\right), \tag{12}$$

where e is the elementary charge (in C), T is the temperature (in degree K), k_b is the Boltzmann's constant, and Γ^0_i is the surface site density of site i, Γ^0_1, Γ^0_2, Γ^0_3 (in sites per nm^2) are the total surface site densities of the three type of sites introduced above (aluminol, silanol, and > Al–O–Si < groups, respectively). The parameters C^f_i where $i = Na^+, H^+$ are the ionic concentrations (in mol L^{-1}), and φ_0 and φ_β are the electrical potentials at the mineral surface (0 plane) and at the β plane, respectively (Figure 2). The resulting mineral surface charge density, Q_0, and the surface charge density in the Stern layer, Q_β (in C m^{-2}), are found by summing the surface site densities of charged surface groups [see *Leroy and Revil*, 2004].

2.2. Complexation of Smectite and Illite

[14] In the case of smectite and illite, the surface site densities are located mainly on the basal plane {001} [*Tournassat et al.*, 2004] (Figure 1b). We use the TLM developed by *Leroy et al.* [2007] to determine the distribution of the counterions at the mineral/water interface of 2:1 clay minerals. In the pH range 6–8, the influence of the hydroxyls surface sites upon the distribution of the counterions at the mineral/water interface can be neglected because the charge density induced by edge sites is small relative to that due to permanent excess of negative charge associated with the isomorphic substitutions inside the crystalline network of the smectite [*Tournassat et al.*, 2004]. We therefore consider only these sites in the model denoted as the "X sites" (see Figure 1). The adsorption of sodium is described by

$$> \mathrm{XNa} \Leftrightarrow > \mathrm{X^-} + \mathrm{Na^+}, K_4, \tag{13}$$

$$\Gamma^0_{\mathrm{XNa}} = \Gamma^0_{\mathrm{X}}\left(\frac{C^f_{\mathrm{Na^+}}}{K_4}\right)\exp\left(-\frac{e\varphi_\beta}{k_bT}\right). \tag{14}$$

Table 1. Optimized TLM Parameters for the Three Main Clay Minerals

Parameters	Kaolinite[a]	Illite[b]	Smectite[b]
K_1 (at 25°C)	10^{-10}	-	-
K_2 (at 25°C)	8×10^{-6}	-	-
K_3 (at 25°C)	5×10^{-2}	-	-
K_4 (at 25°C)	-	0.8	0.8
C_1 (F m^{-2})	1.58	1	1
C_2 (F m^{-2})	0.2	0.2	0.2

[a]From *Leroy and Revil* [2004].
[b]From *Leroy et al.* [2007].

The mineral surface charge density Q_0 (in C m^{-2}) of smectite associated with these sites is considered equal to the ratio between the cation exchange capacity (CEC) of smectite (1 meq g^{-1}) and its specific surface area (800 m^2 g^{-1} [see *Revil et al.*, 1998, and references therein]), which gives a value equal to 0.75 charge nm^{-2} (for illite, a similar analysis yields 1.25 charges nm^{-2}). These values allow the calculation of the surface site densities Γ^0_X and Γ^0_{XNa} knowing the expressions of the mineral surface charge density Q_0 (in C m^{-2}) as a function of the surface site densities [see *Leroy et al.*, 2007].

2.3. Electrical Triple Layer Model

[15] They are three distinct microscopic electric potentials in the inner part of the electrical layer. We note φ_0 the mean potential on the surface of the mineral (Figure 2). The potential φ_β is located at the β plane and φ_d is the potential at the Outer Helmholtz Plane (Figure 2). These potentials are related to each other by a classical capacitance model [*Hunter*, 1981],

$$\varphi_0 - \varphi_\beta = Q_0/C_1 \tag{15}$$

$$\varphi_\beta - \varphi_d = -Q_S/C_2, \tag{16}$$

where C_1 and C_2 (in F m^{-2}) are the (constant) integral capacities of the inner and outer parts of the Stern layer, respectively (Table 1). The parameter Q_S represents the surface charge density in the diffuse layer (see *Leroy and Revil* [2004] for its expression). The global electroneutrality equation for the mineral/water interface is

$$Q_0 + Q_\beta + Q_S = 0. \tag{17}$$

We calculate the potential φ_d by using equations (15) to (17) and the procedure reported by *Leroy and Revil* [2004] and *Leroy et al.* [2007] (the surface charge densities are expressed as a function of the corresponding surface site densities). We use the values of the equilibrium constants K_i and of the capacities C_1 and C_2 reported in Table 1. The system of equations was solved inside two MATLAB routines, one for kaolinite and one for illite and smectite.

[16] The counterions are both located in the Stern and in the diffuse layer. For all clay minerals, the fraction of counterions located in the Stern layer is defined by

$$f_Q = \frac{\Gamma^0_{X_iNa}}{\Gamma^0_{X_iNa} + \Gamma^d_{Na}}, \tag{18}$$

$$\Gamma^d_{Na} \equiv \int_0^\infty \left[C^d_{Na^+}(\chi) - C^f_{Na^+}\right] d\chi = C^f_{Na^+} \int_0^\infty \left\{\exp\left[-\frac{e\varphi(\chi)}{k_bT}\right] - 1\right\} d\chi, \tag{19}$$

$$\varphi(\chi) = \frac{4k_bT}{e} \tanh^{-1}\left[\tanh\left(\frac{e\varphi_d}{4k_bT}\right)\exp(-\kappa\chi)\right], \tag{20}$$

where χ is the distance defined perpendicularly from the interface between the pore water and the solid grain, φ is the electrical potential in the diffuse layer, κ^{-1} is the Debye screening length (in meters) ($2\kappa^{-1}$ corresponds approximately to the thickness of the diffuse layer [see *Revil and Glover*, 1997]), and Γ^d_{Na} is the equivalent surface site density of the counterions in the diffuse layer. The parameter $\Gamma^0_{X_iNa}$ is the surface site density of adsorbed counterions in the Stern layer where X_i corresponds to the > Al–O–Si < surface sites for kaolinite and to the X^- surface sites for illite and smectite. Equation (20) can be found for example in the work of *Hunter* [1981] and is more precise than the classical exponential decay law used in many papers. The superscript d for the concentration and surface site density of sodium refers to the diffuse layer.

[17] As shown by *Leroy and Revil* [2004] and *Leroy et al.* [2007], the previous set of equations can be solved numerically using the parameters given in Table 1 as input parameters. The parameters of Table 1 have been optimized from a number of experimental data, especially zeta potential resulting from electrokinetic measurements and surface conductivity data [see *Leroy and Revil*, 2004; *Leroy et al.*, 2007] and remain unchanged in the present work. The output parameters of the numerical Triple Layer Model (TLM) are the surface site densities in the Stern and diffuse layers and therefore the partition coefficient f_Q. At pH = 5.5, we show in Figures 3 and 4a the surface site densities in the Stern and diffuse layers and the partition coefficient as a function of the salinity for the three different types of clay minerals. A comparison between Figures 4a and 4b shows that clay minerals have a much larger fraction of counterions in the Stern layer by comparison with glass beads at the same salinities. The values of the partition coefficient determined from the present model are also consistent with values determined by other methods, for instance using radioactive tracers [*Jougnot et al.*, 2009] and osmotic pressure [*Gonçalvès et al.*, 2007; *Jougnot et al.*, 2009]. This shows that our electrochemical model is consistent because it can explain a wide diversity of properties. A sensitivity analysis of the TLM model described above was provided by *Leroy and Revil* [2004] and the readers are directed to this paper for further understanding of this model.

3. Modeling the SIP Response

[18] We present the macroscopic electrical conductivity model including both the Maxwell-Wagner polarization and the polarization of the Stern layer of the clay particles. This model accounts for various features that were not accounted for by previous models. They are (1) the fact that the diffuse layer is accounted for inside the pore water for illite and

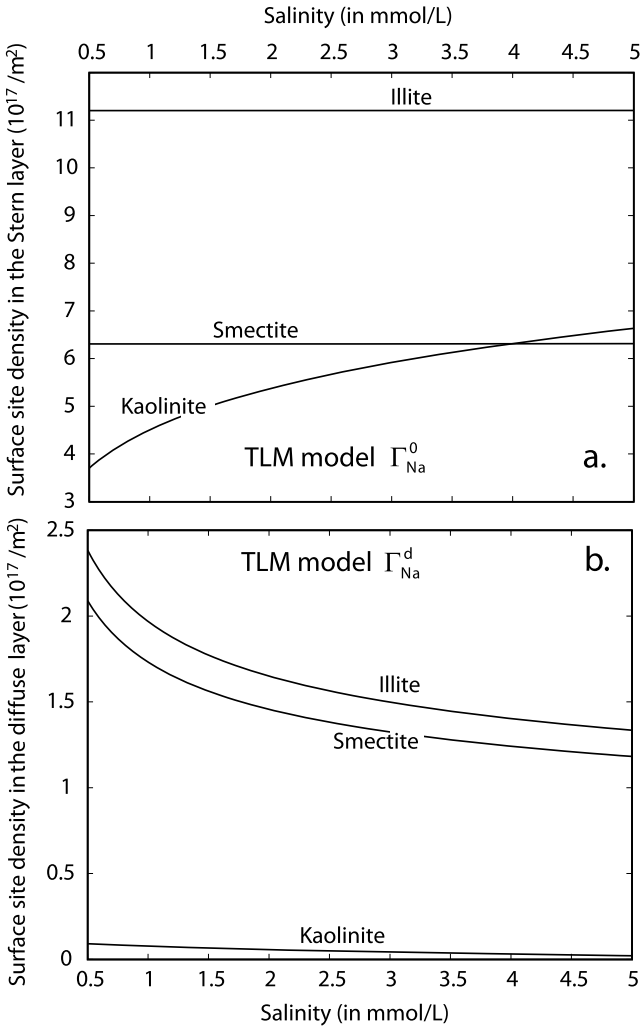


Figure 3. Computation of the surface site densities of counterions (a) in the Stern layer and (b) in the diffuse layer. We use the Triple Layer Model (TLM) described in section 2 (pH = 5.5, NaCl solution).

smectite and has only a contribution in the Maxwell-Wagner polarization (see discussion in the work of *Leroy et al.* [2008]); (2) the grain size distribution is accounted for using a convolution of the Stern polarization model by the particle size distribution (PSD) given either by a log normal distribution, a Cole-Cole distribution, or a composite PSD using a sum of these distributions; and (3) the connection between the TLM model discussed in section 2 and the SIP model is explicit. Therefore temperature, pH, and salinity can be accounted for explicitly.

3.1. A Model for High-Porosity Media

[19] For high-porosity clay media like gels (dilute suspensions of colloidal clays are not considered in the present paper), the differential effective medium (DEM) approach is a suitable tool to obtain a relationship between the electrical conductivity (or permittivity) of the porous material and the conductivity (or permittivity) of its different phases. This is because it takes correctly into account for the mutual polarization effects of the grains in a conductive/dielectric background [*Bruggeman*, 1935; *Hanai*, 1968].

3.1.1. Kaolinite

[20] In the case of kaolinite, we consider that the diffuse layer of the various grains does not fill a large fraction of the pore volume because of the very small specific surface areas of these minerals [*Hassan et al.*, 2006]. The diffuse layer (like the Stern layer) is considered therefore to affect the effective conductivity of the particles only (we will see below that the situation is different for illite and smectite). The DEM approach [*Bruggeman*, 1935; *Hanai*, 1968] yields the following (well-known) relationship between the total conduc-

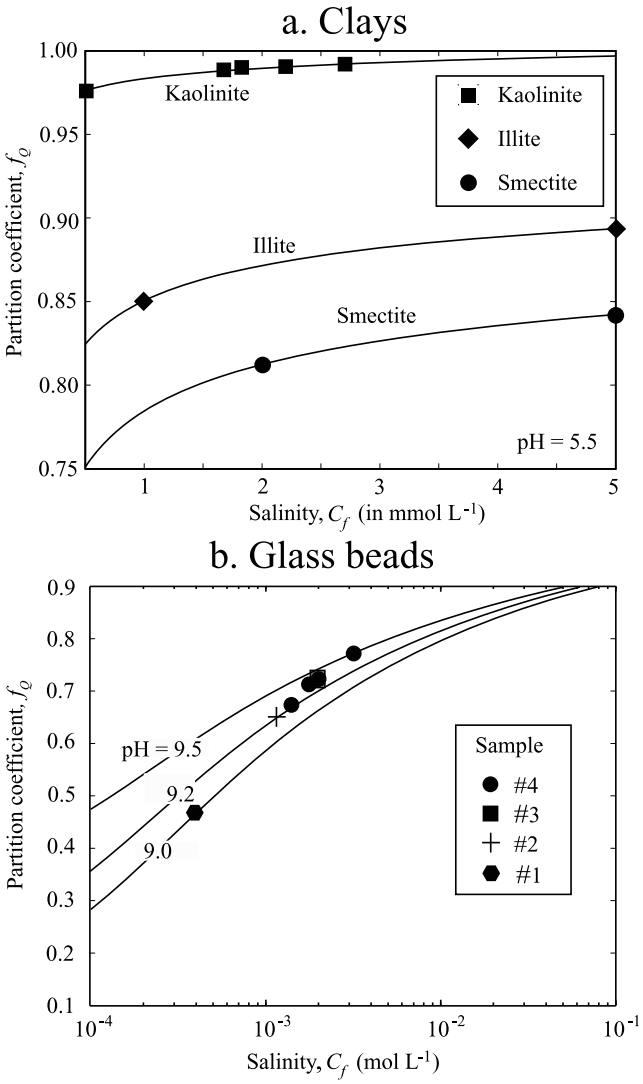


Figure 4. Computation of the partition coefficient for the triple layer model. Note the difference of scales for clays and glass beads. (a) For clays. The symbols represent the values of the partition coefficient corresponding to the spectral induced polarization (SIP) data fitted in this paper. The lines correspond to the results of the TLM model. Kaolinite on one side and illite and smectite on the other show very distinctive values of the partition coefficient. (b) Comparison between the TLM-based computation (plain lines) of the partition coefficient for glass beads and those determined from SIP data using glass beads (filled symbols) [from *Leroy et al.*, 2008].

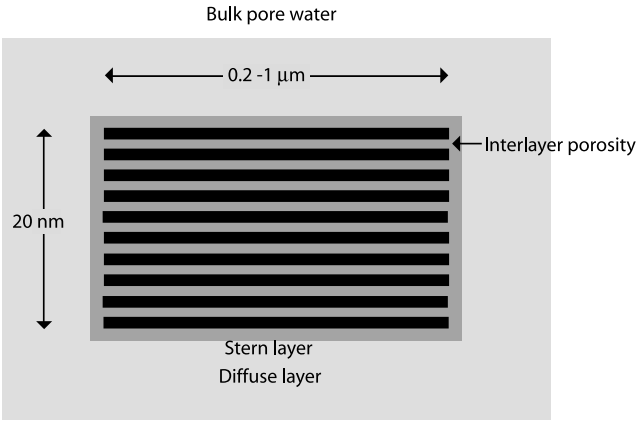


Figure 5. Sketch of a smectite particle. Note the high aspect ratio of the grain. The Stern layer is discontinuous between the basal planes and the lateral faces. For a compacted gel, a particle is usually formed by approximately 10 layers. Using the values given in the main text for the interlayer porosity, this yields a thickness of the particle of ~20 nm while the size of the basal planes is typically equal to ~0.2–1 μm (the thickness of the interlayer pore size in compacted gels is considered equal to three times the diameter of a water molecule, i.e., ~ 8.5 nm).

tivity response of a two-phase mixture consisting of clay particles and pore solution:

$$\sigma^* = \frac{\sigma_f^*}{F}\left(\frac{1-\sigma_s^*/\sigma_f^*}{1-\sigma_s^*/\sigma^*}\right)^m, \tag{21}$$

$$F = \phi_{eff}^{-m}, \tag{22}$$

where m is called the cementation or Archie exponent [*Archie*, 1942], ϕ_{eff} is the effective porosity that is equal to the total connected porosity less the fraction of this total porosity occupied by the electrical double layer, F is the (dimensionless) electrical formation factor, $\sigma^*_f = \sigma_f + i\omega\varepsilon_f$, $\sigma^*_s = \sigma_s + i\omega\varepsilon_s$, and $\sigma^* = \sigma + i\omega\varepsilon$ are the complex electrical conductivity (in S m^{-1}) of the pore water, of the clay particles, and of the porous material, respectively (see Appendix A), and σ_f is the conductivity of the pore water. The value of the cementation exponent depends on the aspect ratio of the clay particles. We found that taking the following set of values (kaolinite, m = 2.0; illite, m = 3; smectite, $m \in \{3, 4\}$) depending on the aspect ratio of the particles works very well (see *Revil et al.* [1998] for an analysis of experimental data and *Mendelson and Cohen* [1982] for theoretical developments). For kaolinite, the value of m can be as low as 1.5 [*Korosak et al.*, 2007]. For smectite, the high value of the cementation exponent is justified by the high aspect ratio of the grains (Figure 5).

[21] The effective porosity is given by $\phi_{eff} = \phi(1 - f)$, where ϕ is the total connected porosity of the medium and f is the fraction of this total porosity occupied by the bound water and the Stern layer,

$$f = \rho_g\left(\frac{1-\phi}{\phi}\right)(d_b S_b + d_l S_l), \tag{23}$$

where S_b and S_l are the specific surface areas of the basal plane (face {001}) and lateral planes (faces {110} and {010}), respectively; d_b and d_l are the thickness on the basal and lateral planes of the Stern layer plus the interlayer thickness for smectite; and ρ_g is the grain density of the clay without the bound water. The values of S_b, S_l, and ρ_g are given in Table 2. For example, considering a clay particle formed by the superposition of N elementary sheets (each of 1 nm), the thickness d_b is given by $d_b = d_{\text{int}} + (d_{\text{Stern}} - d_{\text{int}})/N$ (see Figure 5) where d_{int} (0.42 nm for smectite and 0 nm for illite) is half the thickness of the interlayer pore size (three water molecules, i.e., 0.85 nm [*Tournassat et al.*, 2003]) and d_{Stern} is the thickness of the Stern layer (1 nm, based on recent molecular dynamics simulations from C. Tournassat (personal communication, 2009), which represents half the size of the Stern layer according to *Leroy et al.* [2007]). The thickness to consider on the lateral faces is given by $d_l = d_{Stern}$. For kaolinite, computations show that the effective porosity is very close to the total connected porosity and we will consider that $F \approx \phi^{-m}$. For smectite and illite, f can be as high as 0.4 for compacted low-porosity media [*Leroy et al.*, 2006].

[22] The conductivity of the pore water is given by

$$\sigma_f = \sum_{i=1}^{M} |q_i|\beta_i C_i, \tag{24}$$

where β_i, C_i, and M are the mobility (in m^2 s^{-1} V^{-1}), the concentration of ionic species i in the pore water, and the number of ionic species i in solution, respectively, and $|q_i|$ is the absolute charge of the ions of species i. We introduce also the dimensionless Dukhin number as [see *Bolève et al.*, 2007]

$$\text{Du}^* = \frac{\sigma_s^*}{\sigma_f^*}, \tag{25}$$

where Du* represents the ratio of surface to pore water conductivity. For kaolinite and in the case of the experiments investigated below, the electrical conductivity are never below the isoconductivity point defined by the condition Du $\equiv$ Re(Du*) = 1.

[23] Equation (21) is not very practical because it is of the form $\sigma^* = f(F, \sigma^*_f, \sigma^*_s, \sigma^*)$. Because Du < 1, equation (21) can be written in a closed form as [*Revil et al.*, 1998, *Revil*, 2000]

$$\sigma^* \approx \frac{\sigma_f^*}{F}\left[F\text{Du}^* + \frac{1}{2}(1-\text{Du}^*) \cdot\left(1-\text{Du}^* + \sqrt{(1-\text{Du}^*)^2 + 4F\text{Du}^*}\right)\right]. \tag{26}$$

Table 2. Specific Surface Areas and Grain Density of Clays

Clay	S_b (m^2 g^{-1})	S_l (m^2 g^{-1})	ρ_g (kg m^{-3})
Kaolinite	17[a]	3[a]	2600[c]
Illite	133[a]	38[a]	2800[c]
Smectite	780[b]	20[b]	2700[c]

[a]From *Hassan et al.* [2006].
[b]From *Tournassat et al.* [2003].
[c]Mass density of the grains obtained from the crystallographic unit cell.

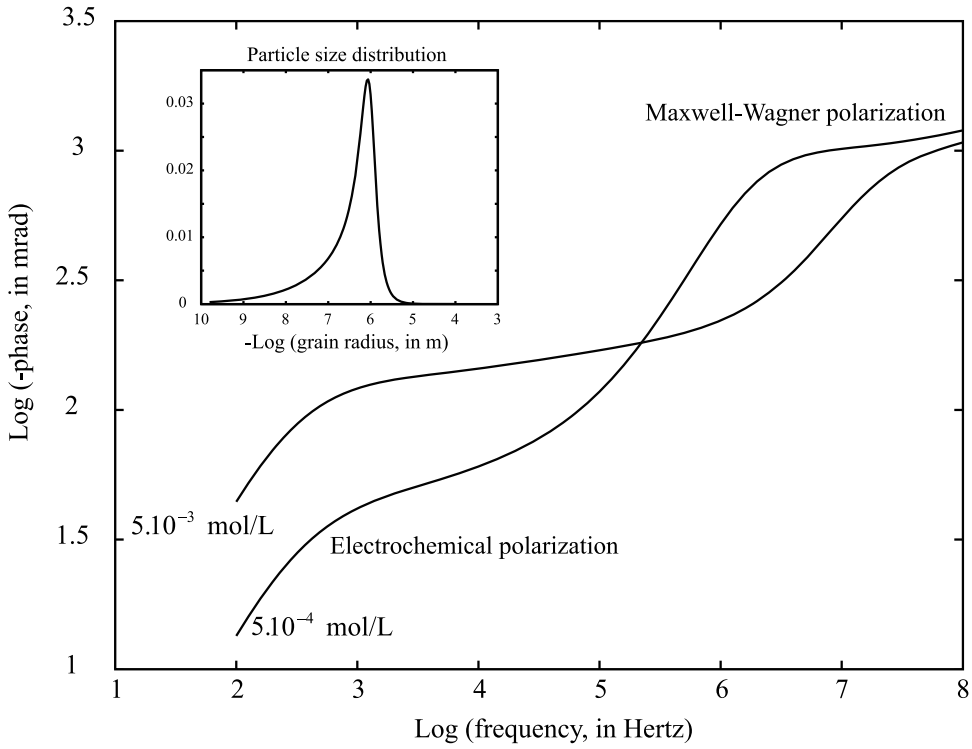


Figure 6. Prediction of the phase as a function of the frequency for kaolinite at two salinities (input parameters given in Table 3). We show also the domains dominated by the electrochemical polarization at low frequencies and the Maxwell-Wagner polarization at high frequencies.

The complex conductivity can be also written as (see Appendix A)

$$\sigma^* = \sigma_{eff} + i\omega\varepsilon_{eff}, \tag{27}$$

$$\sigma_{eff} = \mathrm{Re}\left(\sigma^*\right), \tag{28}$$

$$\varepsilon_{eff} = \mathrm{Im}\left(\sigma^*/\omega\right). \tag{29}$$

The phase of the complex conductivity response is defined by

$$\Theta = -\tan^{-1}\left(\omega\varepsilon_{eff}/\sigma_{eff}\right). \tag{30}$$

[24] For kaolinite, there are two contributions to the surface conductivity. The first contribution is related to the electromigration of the counterions in the diffuse layer. The second contribution is associated with the electromigration of the counterions in the Stern layer. In our model, only this second contribution is frequency dependent [*Leroy et al.*, 2008] because the diffuse layer is continuous at the scale of the porous continuum. We will see in section 5, however, that another polarization mechanism is at play at very low frequencies (<1 Hz) and could involve the polarization of the diffuse layer inside the pore space.

[25] The total surface conductivity of kaolinite particles in the case of a binary symmetric electrolyte (like NaCl or KCl) is given by [*Leroy et al.*, 2008]

$$\sigma_s = \frac{2}{a}\left(\Sigma_S^0 + \Sigma_S^\infty\right) - \frac{2}{a}\frac{\Sigma_S^\infty}{(1+i\omega\tau_0)}, \tag{31}$$

$$\Sigma_S^\infty = \beta_i^S e\Gamma_i^0, \tag{32}$$

$$\Sigma_S^0 = \beta_i e\Gamma_i^d, \tag{33}$$

where Σ_S^∞ represents the contribution of the Stern layer at high frequencies, Σ_S^0 represents the contribution of the diffuse layer, and a is the radius of the grain (in meters). Equation (31) is similar to equation (6) from *De Lima and Sharma* [1992]. The relaxation time τ_0 (in seconds) is determined from the value of the diffusion of the counterions in the Stern layer D_i^S (in $m^2\ s^{-1}$), which are related to the ionic mobilities by the Nernst-Einstein relationship [*Leroy et al.*, 2008]. In addition, we have $\sigma^*_s = \sigma_s + i\omega\varepsilon_s$ where ε_s represent the effective permittivity of the grain, including the effect of the electrical double layer and the bound water.

[26] The model prediction for a kaolinite sample is shown in Figure 6 (the input parameters are given in Table 3). The Maxwell-Wagner polarization dominates at high frequencies while the polarization of the Stern layer dominates at

Table 3. Input Parameters for the Synthetic Model of Kaolinite Saturated by a NaCl Solution

Parameter	$C_f = 5 \times 10^{-4}$ mol L^{-1}	$C_f = 5 \times 10^{-3}$ mol L^{-1}
m	2.0	2.0
ϕ	0.6	0.6
c	0.7	0.7
Γ^0_{Na} [a] (nm^{-2})	0.35	0.66
Γ^d_{Na} [a] (nm^{-2})	0.009	0.0021
f_Q [b]	0.975	0.995
d (μm)	1	1
β^S_{Na} (m^2 s^{-1} V^{-1})	5.19×10^{-8}	5.19×10^{-8}

[a] From the TLM model at the given salinity (NaCl).
[b] Determined using $f_Q = \Gamma^0_{Na}/(\Gamma^0_{Na} + \Gamma^d_{Na})$.

low frequencies. However, it is difficult to separate this polarization from the Maxwell-Wagner polarization because they are overlapping in the frequency domain and because the conduction in the Stern layer influences both processes.

3.1.2. Illite and Smectite

[27] In the case of illite and smectite at low salinity (typically $< 10^{-2}$ mol L^{-1}), we consider that the diffuse layer of the various particles is continuous at the scale of the representative elementary volume but not the Stern layer. The equations we used to characterize the complex conductivity of the medium are the same than previously taking $\overline{\sigma}_f$ instead of σ_f for the pore water conductivity and $\overline{\sigma}_s$ instead of σ_s for the surface conductivity of the clay particles. The conductivity of the pore water is given by [*Revil and Linde*, 2006]

$$\overline{\sigma}_f = \sum_{i=1}^{M} |q_i| \beta_i \overline{C}_i, \tag{34}$$

where $\overline{C}_i$ is the concentration of ionic species i in the diffuse layer. As explained by *Leroy et al.* [2007], the composition of the pore water of a clay-rich material (with illite and smectite) differs from the composition of the pore water of a neutral electrolyte directly in contact and in equilibrium with the clay material. The concentration of cations is higher in the pore space than in the reservoir and the concentration of anions is lower. *Leroy et al.* [2007] and *Jougnot et al.* [2009] used the generalized Donnan equilibrium model developed by *Revil and Linde* [2006] to account for this effect.

[28] At low salinity and assuming that one cation (like K^+ or Na^+) is the dominant ionic species in the pore space, we have the approximation

$$\overline{\sigma}_f \approx \beta_{(+)} \overline{Q}_V, \tag{35}$$

where $\overline{Q}_V$ (in C m^{-3}) is the volumetric charge density of the pore water. From the definition of the partition coefficient f_Q (see section 2), we have $\overline{Q}_V = (1 - f_Q) Q_V$ [*Revil and Leroy*, 2004] where Q_V represents the total bulk charge density corresponding to the excess of charge per unit pore volume of the porous material,

$$Q_V = \rho_g \left(\frac{1 - \phi}{\phi} \right) CEC, \tag{36}$$

where ρ_g is the grain density (in kg m^{-3}) (Table 2) and the CEC is the cation exchange capacity (in meq g^{-1}, 1 meq g^{-1} = 96320 C kg^{-1}) of the clay minerals (an arithmetic average can be used for a mixture). At low salinities, equation (35) implies that the conductivity of the pore water inside a clay assemblage (or a clay rock) does not depend explicitly on the salinity of the water contained in a porous and permeable reservoir in contact and in equilibrium with the clay material. What is the effect on the Dukhin number in this case? The dimensionless Dukhin number is

$$\mathrm{Du}^* = \frac{\overline{\sigma}^*_s}{\overline{\sigma}^*_f}, \tag{37}$$

(Du* represents the ratio of surface to pore water conductivity). At low salinities, $\overline{\sigma}_f \approx \beta_{(+)} \overline{Q}_V$ and the

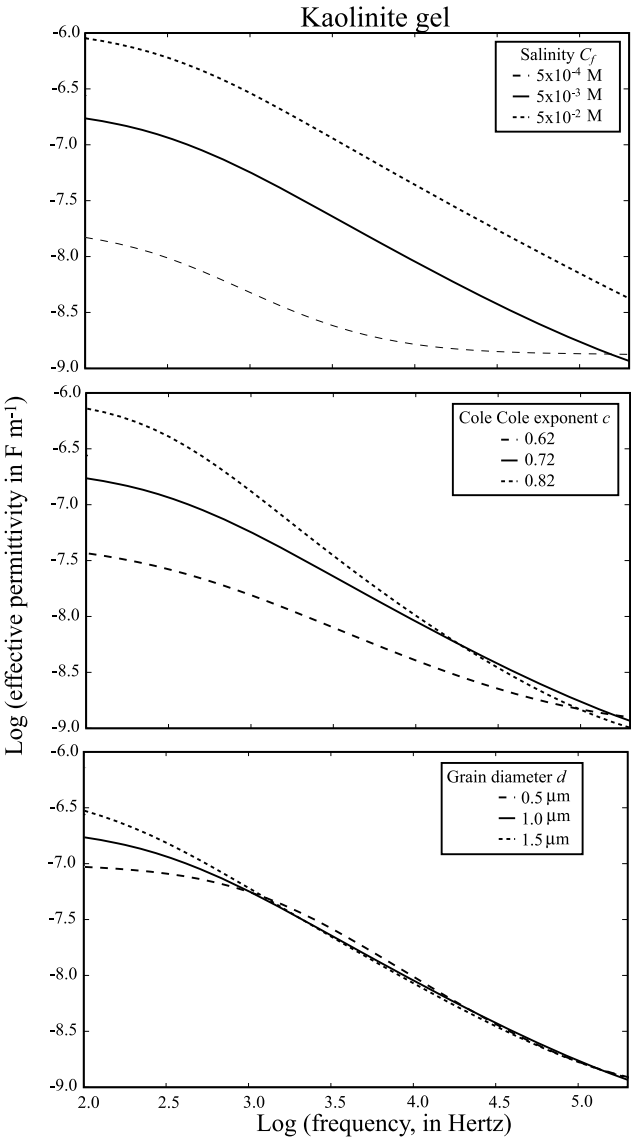


Figure 7. Sensitivity analysis for a kaolinite gel for different values of the Cole-Cole exponent and mean grain diameter assuming that the grain size distribution is given by a Cole-Cole distribution (see other parameters in Table 4).

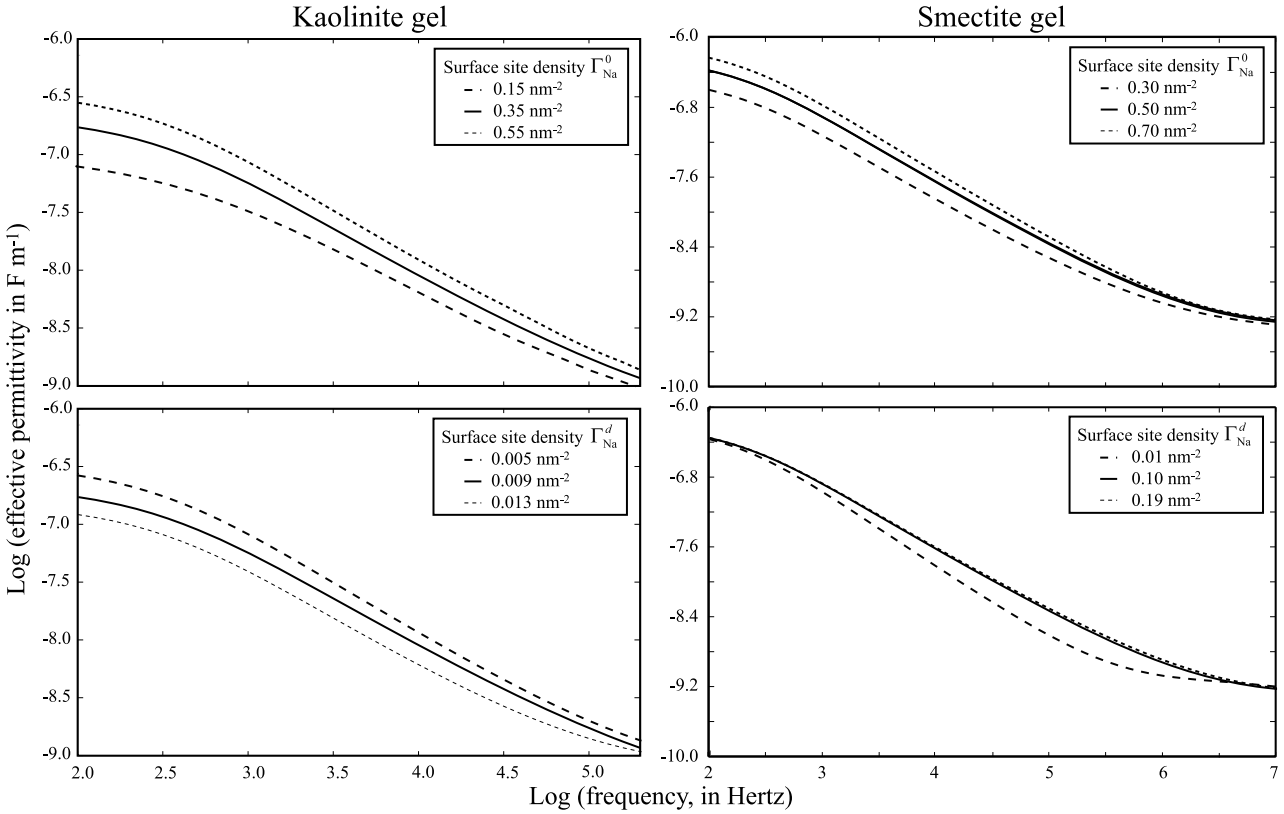


Figure 8. Sensitivity analysis for kaolinite and smectite for different values of the salinity, cation exchange capacity (CEC), and surface site densities in the Stern and diffuse layers (see other parameters in Table 4).

real part of the Dukhin number Du = Re(Du*) in the case of sorbed sodium is given by

$$\mathrm{Du} = \frac{2e\beta^S_{\mathrm{Na}}\Gamma^0_{\mathrm{Na}}}{a\beta_{\mathrm{Na}}\overline{Q}_V}. \tag{38}$$

[29] The mobility of the sodium in the pore water β_{Na} is ten times larger in the diffuse layer and in the free pore water than in the Stern layer (β^S_{Na}) for illite and smectite. This yields Du $\ll$ 1. For example, using f_Q = 0.8, CEC = 1 meq g^{-1} (1 meg g^{-1} = 96,320 C kg^{-1}), $\Gamma^0_{\mathrm{Na}} = 10^{18}$ sites m^{-2}, ϕ = 0.5, ρ_g = 2700 kg m^{-3}, and $a = 10^{-7}$ m (typical of a smectite particle at low salinity), we obtain Du $\sim 6.2 \times 10^{-3}$. Consequently and quite surprisingly, the electrical conductivity data are never below the isoconductivity point (corresponding to the condition Du > 1 [see *Crespy et al.*, 2007]). Therefore equation (26) can be used with σ_f replaced by $\overline{\sigma}_f$.

[30] Finally, the conductivity of an illite and smectite particle coated by the Stern layer is

$$\overline{\sigma}_s = \frac{2\Sigma^\infty_S}{a}\left(\frac{i\omega\tau_0}{1+i\omega\tau_0}\right), \tag{39}$$

$$\Sigma^\infty_S = e\beta^S_i\Gamma^0_i. \tag{40}$$

In equations (39) and (40), surface conductivity comprises only the Stern layer because the diffuse layer is accounted for in the pore space (inside $\overline{\sigma}_f$). Therefore surface conductivity associated with the Stern layer is negligible by comparison with the pore water conductivity that is due to the diffuse layer.

[31] The complex electrical conductivity of the entire mixture composed of N different grain radii is determined by [*Lesmes and Morgan*, 2001]

$$\sigma^*_s = \int_0^\infty f(a')\sigma^*_s(a', \omega)da', \tag{41}$$

$$\sigma^*_s = \sum_{i=1}^{N} f(a_i)\sigma^*_s(a_i, \omega), \tag{42}$$

where a_i is the particle radius of the grain i, and $f(a_i)$ represents the discretized version of the particle size distribution (PSD) $f(a)$. The total grain volume distribution is normalized according to

$$\int_0^\infty f(a')da' = 1, \tag{43}$$

$$\sum_{i=1}^{N} f(a_i) = 1. \tag{44}$$

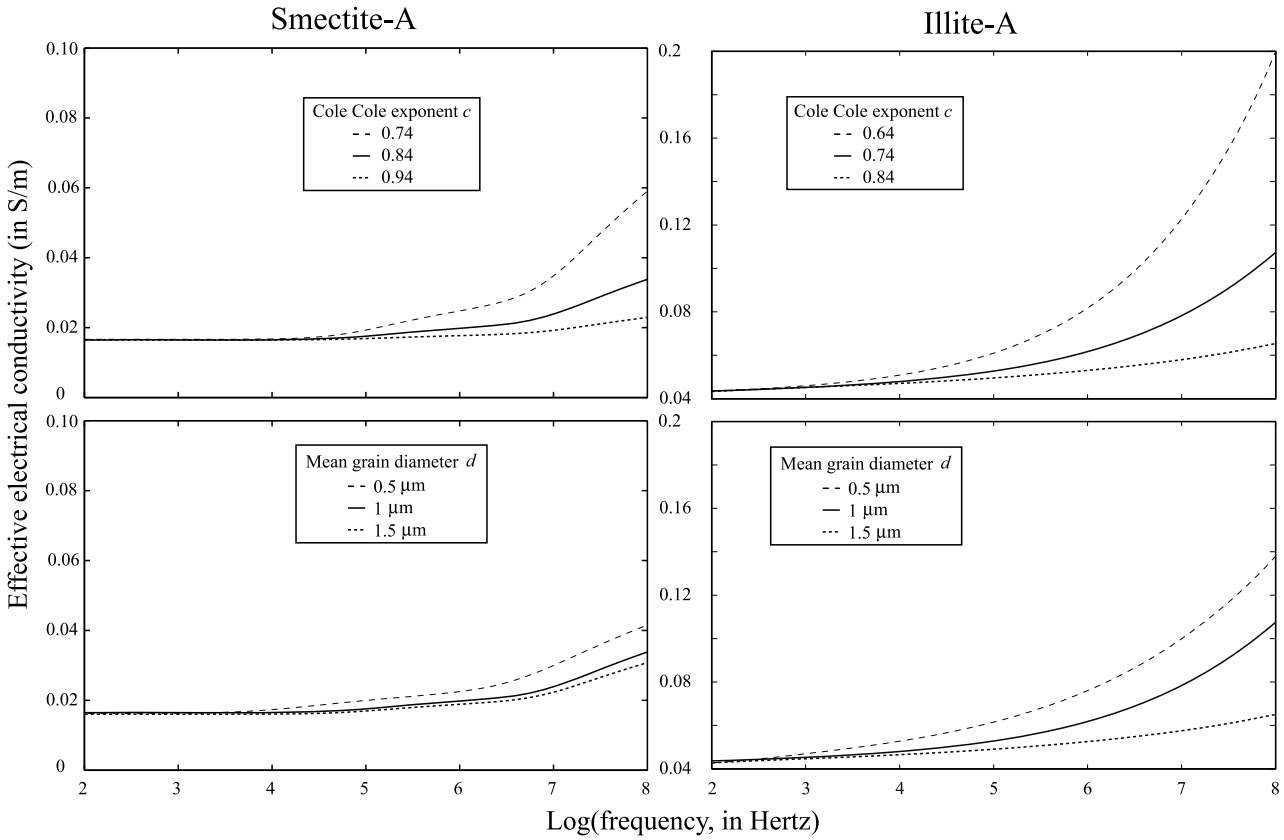


Figure 9. Sensitivity analysis for smectite and illite for different values of the Cole-Cole exponent and mean grain diameter assuming that the grain size distribution is given by a Cole-Cole distribution (see other parameters in Table 8).

This behavior can also be connected with the so-called Cole-Cole distribution. In dealing with the dispersive complex surface conductivity function, we can write

$$\sigma_s^*(\omega) = \sigma_s^\infty + \left(\sigma_s^0 - \sigma_s^\infty\right) \int_0^\infty \frac{g(\tau)}{1 + i\omega\tau} d\tau, \tag{45}$$

where σ_s^∞ is the high-frequency surface conductivity and σ_s^0 is the low-frequency surface conductivity (low and high frequencies are defined with respect to the critical angular frequency $\omega_c = 1/\tau$). Both σ_s^∞ and σ_s^0 are real parameters. The function $g(\tau)$ represents the distribution of the relaxation times. It is normalized such that

$$\int_0^\infty g(\tau) d\tau = 1. \tag{46}$$

[32] The model predictions for kaolinite, smectite, and illite are shown in Figures 7 to 10. In Figures 7 to 10, we keep all the parameters as constant except one to observe the sensitivity of the effective permittivity and conductivity versus the frequency. Figure 7 shows that the effective permittivity of a kaolinite gel presents a very high sensitivity to the Cole-Cole exponent. The higher the Cole-Cole exponent (narrower distribution of grain size) and the mean diameter, the higher is the effective permittivity at low frequency. According to Figure 8, the surface site densities of counterions in the Stern and diffuse layers influence both the effective permittivity, especially for kaolinite. The effective permittivity of smectite is not very sensitive to the surface site density of counterions in the diffuse layer.

[33] Figure 9 presents the effective conductivity of smectite and illite. The effective conductivity is very sensitive to both the Cole-Cole exponent and to the mean grain diameter. The lower the Cole-Cole exponent (broader distribution of grain size) and the mean diameter, the higher is the electrical response at high frequency. Indeed, the conductivity is inversely proportional to the grain diameter (term "$2/a$" in equations (31) and (39)). According to Figure 10, the surface site density of counterions in the diffuse layer influences the conductivity response at all the frequencies (constant shift of the electrical response). Indeed, in our model, the polarization of the diffuse layer is not frequency dependent. The frequency dependence of the Stern layer conductivity has a greater influence for kaolinite than in the case of smectite. The surface site densities of counterions in the Stern and diffuse layers have opposite contributions to the electrical response.

3.2. A Model for Clay Rocks

[34] We develop now a spectral induced polarization model for a low-porosity clay rock or a shale. The mineral matrix of these materials is formed by clay minerals in

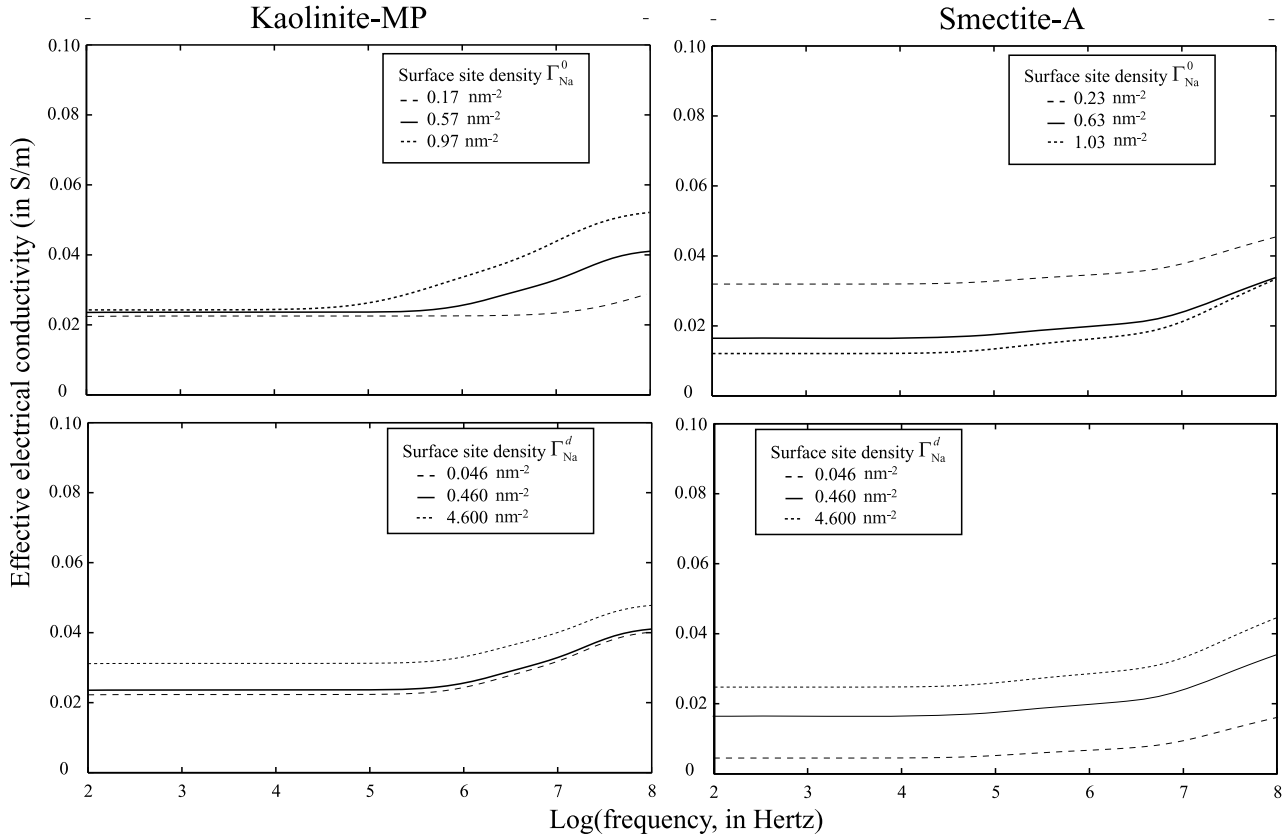


Figure 10. Sensitivity analysis for kaolinite and smectite for different values of the surface site densities in the Stern and diffuse layers (see other parameters in Table 8).

which some grains of silica and carbonate are immersed (Figure 11). The polarization of clay materials requires the development of a specific model because the thickness of the electrical diffuse layer is on the same order of magnitude than the size of the pores and because the clay particles are in close contact with each other.

[35] For a low-porosity or compacted clay assemblage, *Revil and Linde* [2006] have developed recently a new conductivity model incorporating both the conduction in the Stern and diffuse layer. They model was based on a volume-averaging of the local Nernst-Planck equation. Equation (176) of *Revil and Linde* [2006] yields

$$\sigma_c^* = \frac{1}{F_c}\left[\sigma_f^* + (F_c - 1)\sigma_s^*\right], \tag{47}$$

where $F_c = \phi_c^{-m_c}$ is the electrical formation factor of the clay assemblage or clay matrix, ϕ_c is the porosity of the clay assemblage, m_c is the cementation exponent of the clay assemblage, and $\sigma^*_f = \overline{\sigma}_f + i\omega\varepsilon_f$, $\sigma^*_s = \overline{\sigma}_s + i\omega\varepsilon_s$, and $\sigma_c^* = \sigma_c + i\omega\varepsilon_c$.

[36] A clay rock is a sedimentary rock that contains not only a matrix of clay particles with their own porosity but also silica and/or carbonates grains that are immersed in this matrix. In this case, we can follow the scheme used by *Revil* [2000]. A granular model is usually modeled with the DEM approach by assuming that the assemblage of grains floats in a background water. We can replace the background water by the clay matrix. In this case, the change of variables is $\sigma^*_s \rightarrow i\omega\varepsilon_s$ (the coarse grains are assumed to be insulating and the effect of surface conductivity of these

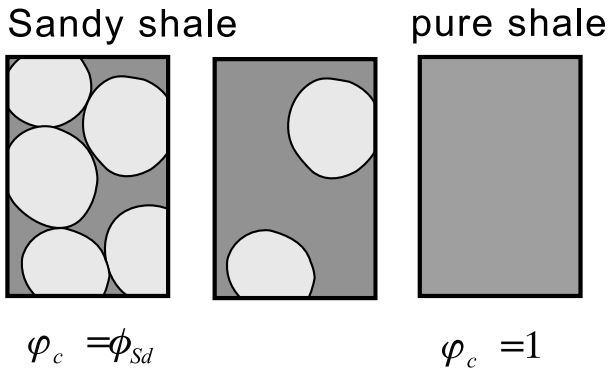


Figure 11. Sandy or silty shales are formed by silt and/or sand grains immersed into a clayey matrix with its own porosity. The volumetric clay content ϕ_c is bounded by two values corresponding to two limiting cases. The first one is the case where a silt (or a sand) is completely infiltrated by clays with their own porosity. The second limiting case is the (usually fictitious) case of a pure shale without silt or sand grains immersed in the clay matrix.

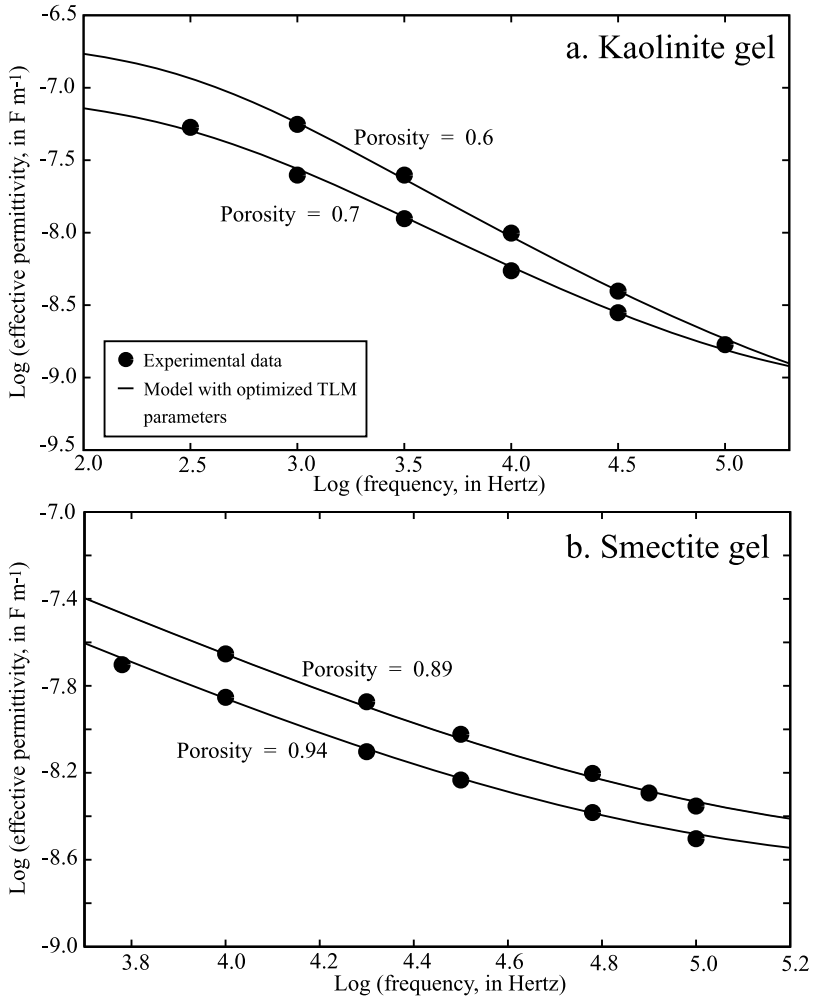


Figure 12. Comparison between the experimental data of *Lockhart* [1980a, 1980b] and the prediction of the differential effective medium approach for the effective permittivity (expressed in F m^{-1}) using the TLM parameters of Table 4 at the salinity and pH (~5.5) of the pore water solution. (a) Kaolinite. (b) Smectite.

Table 4. Values of the Model Parameters Used to Fit the Experimental Data of *Lockhart* [1980a, 1980b] Using NaCl Solutions at 0.5×10^{-3} mol L^{-1} for the Kaolinite Gel[a]

Parameter	Kaolinite-1	Kaolinite-2	Smectite-1	Smectite-2
m	2.0	2.0	4.0	4.0
C_f (mol L^{-1})	$(5 \pm 2) \times 10^{-4}$	$(5 \pm 2) \times 10^{-4}$	-	-
ϕ[b]	0.70	0.60	0.94	0.88
c[c]	0.68 ± 0.05	0.72 ± 0.05	0.60 ± 0.10	0.68 ± 0.05
Γ^0_{Na} (nm^{-2})	0.35 ± 0.05	0.35 ± 0.05	0.50 ± 0.10	0.50 ± 0.10
Γ^d_{Na} (nm^{-2})	$(9 \pm 2) \times 10^{-3}$	$(9 \pm 2) \times 10^{-3}$	0.10 ± 0.05	0.10 ± 0.05
f_Q[d]	0.975	0.975	0.84	0.84
d[e] (μm)	1.0 ± 0.7	1.0 ± 0.3	0.4 ± 0.3	0.4 ± 0.2
β^S_{Na} (m^2 s^{-1} V^{-1})	5.19×10^{-8}	5.19×10^{-8}	0.52×10^{-8}	0.52×10^{-8}

[a]The uncertainties are twice the standard deviations (pH = 5.5).
[b]Determined using the grain density and the quantity of clays (in g L^{-1}) in the mixture.
[c]Value of the Cole-Cole exponent.
[d]Determined using $f_Q = \Gamma^0_{Na}/(\Gamma^0_{Na} + \Gamma^d_{Na})$; $(9 \pm 2) \times 10^{-3}$.
[e]Default size of the kaolinite and smectite particles (see Figures 1 and 5).

Table 5. TLM Computations of the Surface Site Densities of Sodium in the Stern and Diffuse Layers Using the Parameters From Table 1[a]

	Salinity C_f (mol L^{-1})			
	0.5×10^{-3}	1×10^{-3}	5×10^{-3}	10×10^{-3}
		Kaolinite		
Γ^0_{Na} (nm^{-2})	0.35	0.45	0.66	0.77
Γ^d_{Na} (nm^{-2})	0.009	0.0065	0.0021	~0
f_Q[b]	0.975	0.985	0.995	~1
		Illite		
Γ^0_{Na} (nm^{-2})	1.12	1.12	1.12	1.12
Γ^d_{Na} (nm^{-2})	0.238	0.197	0.133	0.115
f_Q[b]	0.82	0.85	0.89	0.91
		Smectite		
Γ^0_{Na} (nm^{-2})	0.631	0.631	0.631	0.632
Γ^d_{Na} (nm^{-2})	0.209	0.173	0.118	0.102
f_Q[b]	0.75	0.785	0.84	0.86

[a]We consider a pH equal to 5.5 for kaolinite [see *Lockhart*, 1980b] while the results are independent of the pH of the solution for illite and smectite. The surface concentrations Γ^0_{Na} and Γ^d_{Na} correspond to the number of counterions per nm^2 in the Stern and diffuse layers, respectively.
[b]Determined from $f_Q = \Gamma^0_{Na}/(\Gamma^0_{Na} + \Gamma^d_{Na})$.

grains can be neglected here with respect to the conductivity of the clay particles), $\sigma^*_f \rightarrow \sigma^*_c$ (the conductivity of the water is replaced by the conductivity of the clay assemblage), and $1/F \rightarrow \varphi_c^2$, φ_c is the volumetric clay content. This yields

$$\sigma^* = \sigma^*_c \varphi_c^2 \left[\varphi_c^{-2} \mathrm{Du}^* + \frac{1}{2}\left(1 - \mathrm{Du}^*\right) \cdot \left(1 - \mathrm{Du}^* + \sqrt{\left(1 - \mathrm{Du}^*\right)^2 + 4\varphi_c^{-2}\mathrm{Du}^*}\right)\right], \quad (48)$$

$$\mathrm{Du}^* = \frac{i\omega\varepsilon_s}{\sigma^*_c}. \quad (49)$$

The apparent formation factor of the porous material is obtained by taking Du* = 0. This yields

$$\frac{1}{F_a} = \varphi_c^2 \phi_c^{m_c}. \quad (50)$$

The porosity ϕ of the clay rock is given by

$$\phi = \varphi_c \phi_c. \quad (51)$$

Table 6. Comparison Between the Pore Fluid Conductivities Used in the SIP Model and Those Measured by *Arulanandan* [1969][a]

Sample	Model	Measured
Kaolinite-121	2.9×10^{-2}	2.0×10^{-2}
Kaolinite-MP	3.5×10^{-2}	2.4×10^{-2}
Kaolinite-R	4.0×10^{-2}	4.5×10^{-2}
Kaolinite-UF	2.2×10^{-2}	2.4×10^{-2}
Illite-A	5.6×10^{-1}	7.2×10^{-2}
Smectite-A	6.9×10^{-1}	2.8×10^{-2}

[a]Pore fluid conductivities used in the SIP model are determined from equation (24) for kaolinite and equation (35) for smectite.

Table 7. Experiments Made by *Arulanandan* [1969][a]

Parameter	Kaolinite-121	Kaolinite-MP	Kaolinite-R
m	2.0	2.0	2.0
C_f (mol L^{-1})	$(1.8 \pm 0.5) \times 10^{-3}$	$(2.7 \pm 0.5) \times 10^{-3}$	$(2.2 \pm 0.5) \times 10^{-3}$
ϕ[b]	0.65	0.70	0.60
c	-	-	-
Γ^0_{Na} (nm^{-2})	0.52 ± 0.10	0.57 ± 0.10	0.55 ± 0.10
Γ^d_{Na} (nm^{-2})	$(6 \pm 5) \times 10^{-3}$	$(4.6 \pm 4.0) \times 10^{-3}$	$(5.4 \pm 5.0) \times 10^{-3}$
f_Q[c]	0.99	0.99	0.99
d (μm)	-	-	-
β^S_{Na} (m^2 s^{-1} V^{-1})	5.19×10^{-8}	5.19×10^{-8}	5.19×10^{-8}

[a]NaCl, pH ~5.5.
[b]Determined from the water content and the mass density of the clay particles.
[c]Determined from $f_Q = \Gamma^0_{Na}/(\Gamma^0_{Na} + \Gamma^d_{Na})$.

Using equations (50) and (51) with $m_c = 2$, we obtain $F_a = \phi^{-2}$, which is the classical Archie law between the formation factor and the porosity with a cementation exponent equal to 2.

4. Comparison With Experimental Data

4.1. High-Porosity Gels

[37] We compare the SIP model described above in section 3 to the experimental data obtained by *Lockhart* [1980a, 1980b]. In absence of information on the particle size distribution, we use a Cole-Cole model (see Appendix B). To fit the data, different tests were performed for the value of the mobility of the counterions in the Stern layer. Finally, we consider that for kaolinite, the mobility of the counterions in the Stern layer is equal to the mobility of the counterions in the bulk pore water [see *Leroy et al.*, 2008]. Indeed, the surface charge properties of kaolinite and glass beads depends both on the presence of hydroxyl surface (silanol and aluminol) groups. This is not the case of illite and smectite which have both permanent structural charges on their basal surface.

[38] Figure 12a shows a comparison between our model and the data for Kaolinite-1 and Kaolinite-2 (data from *Lockhart* [1980b]). The data correspond to a plot of the

Table 8. Experiments Made by *Arulanandan* [1969][a]

Parameter	Kaolinite-UF	Illite-A	Smectite-A
m	2.0	2.5	3.0
C_f (in mol L^{-1})	$(1.7 \pm 0.5) \times 10^{-3}$	-	-
ϕ	0.81[b]	0.35[c]	0.30[c]
c	-	0.74 ± 0.05	0.84 ± 0.05
Γ^0_{Na} (nm^{-2})	0.45 ± 0.10	0.12 ± 0.02	0.63 ± 0.20
Γ^d_{Na} (nm^{-2})	$(6 \pm 5) \times 10^{-3}$	0.13 ± 0.02	0.14 ± 0.02
f_Q[d]	0.985	0.895	0.82
d (μm)	-	1 ± 0.5	1 ± 0.5
β^S_{Na} (m^2 s^{-1} V^{-1})	5.19×10^{-8}	0.52×10^{-8}	0.52×10^{-8}

[a]NaCl, pH ~5.5.
[b]Determined from the water content and the mass density of the clay particles.
[c]Using 10 sheets per particle, three sorbed water layers for the interlayer porosity, and 1 nm for the thickness of the Stern layer.
[d]Determined from $f_Q = \Gamma^0_{Na}/(\Gamma^0_{Na} + \Gamma^d_{Na})$.

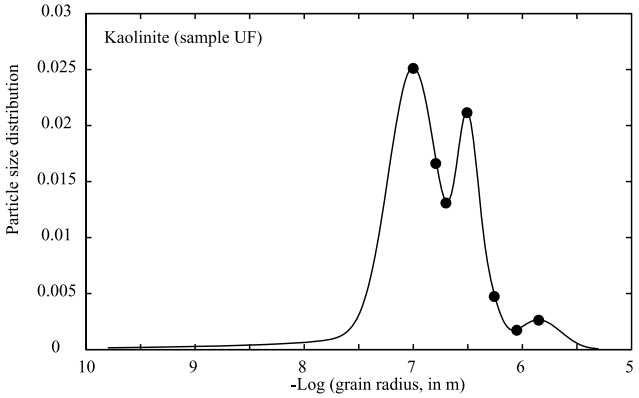


Figure 13. Example of particle size distribution (PSD) corresponding to the kaolinite core sample UF. Experimental data from *Arulanandan* [1969]. The PSD is fitted by the sum of two log normal distributions and a Cole-Cole distribution.

effective permittivity as a function of the frequency. We fit the data by optimizing the density of the counterions in the Stern layer, Γ^0_{Na}, and in the diffuse layer, Γ^d_{Na}, by using the Simplex algorithm. The optimized values of Γ^0_{Na} and Γ^d_{Na} are reported in Table 4. In Table 5, we use the TLM model presented in section 2 and the TLM parameters of Table 1, to compute the values of Γ^0_{Na} and Γ^d_{Na}. They are remarkably consistent with the values optimized by using the SIP data. The value of $f_Q = 0.975$ is the same from the model and the data.

[39] The same work is performed for the SIP data of two gels of two homoionic Na-smectites [*Lockhart*, 1980a]. The petrophysical properties of the two denser smectite gels discussed by *Lockhart* [1980a] are reported in Table 4. Taking $n = 3$ for the number of hydration layers in the interlayer pore space, and considering that a particle is formed of four sheets, we can determine the value of the effective porosity. For the particle size distribution, we use a Cole-Cole distribution (Appendix B). The comparison between the SIP model and the experimental data is shown in Figure 12b. The mobility of sodium in the Stern layer is considered to be ten times smaller than the mobility of sodium in the bulk pore water [*Revil et al.*, 1998]. The conductivity of the pore water is determined using the low salinity limit $\overline{\sigma}_f = \beta_{(+)}\overline{Q}_V$. To determine the value of $\overline{Q}_V$, the CEC is taken equal to the value of a smectite single sheet divided by the number of sheets forming the particle (four in the present case). Therefore the effective CEC is equal to 0.25 meq g^{-1}. In addition, because of the high aspect ratio of the smectite particles (see Figure 5), we consider that $m = 4.0$. The best fits for Γ^0_{Na} and Γ^d_{Na} are reported in Table 4. In Table 5, we used the TLM model presented in section 2 with the TLM parameters of Table 1 to compute the values of Γ^0_{Na} and Γ^d_{Na}. These results are consistent.

4.2. Low-Porosity Gels

[40] We use the data of *Arulanandan* [1969] for compacted kaolinite, illite, and smectite gels. For all the samples, the pore fluid conductivity of the clay samples has been measured independently by the author. They are reported in Table 6. Tables 7 and 8 provide the values of the parameters used in the model.

[41] For kaolinites (four samples), the particle size distributions are known and used for the SIP models by fitting

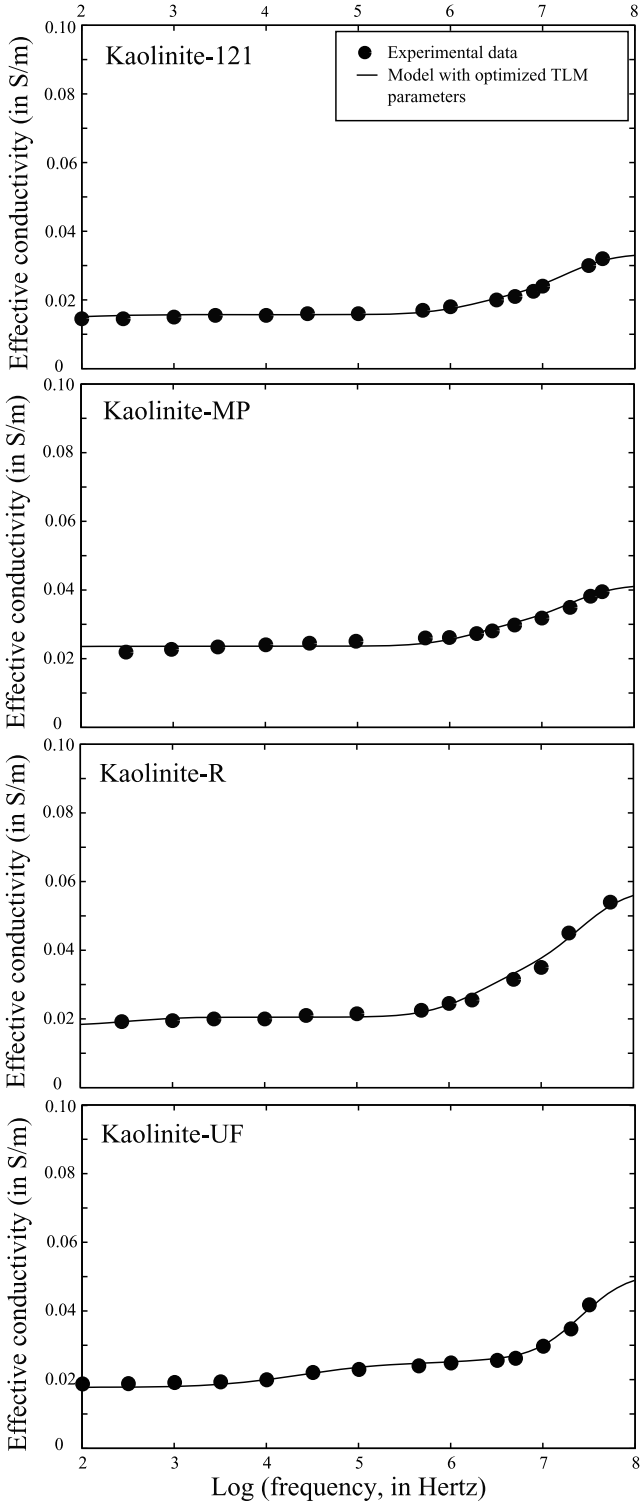


Figure 14. Comparison between the data of *Arulanandan* [1969] and the prediction of the differential effective medium approach for kaolinite concerning the effective conductivity (in S m^{-1}) using the measured PSD.

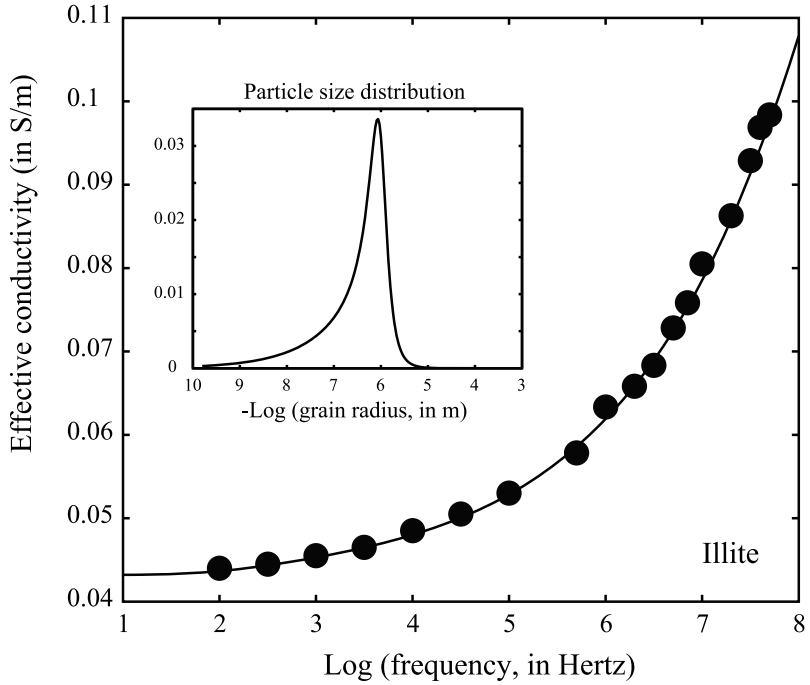


Figure 15. Comparison between the experimental data of *Arulanandan* [1969] and the prediction of the differential effective medium approach concerning the effective conductivity (in S m^{-1}) for illite. The PSD being unknown, we use a Cole-Cole distribution for the PSD (see the insert and Table 8).

them with a sum of log normal and Cole-Cole distributions (see, for example, Figure 13). The log normal distribution is given by

$$f(a) = \frac{1}{\sqrt{2\pi}\hat{\sigma}} \exp\left\{-\left[\frac{\log(a/a_0)}{\sqrt{2}\hat{\sigma}}\right]^2\right\}, \qquad (52)$$

where a_0 is the peak of the particle size distribution and $\hat{\sigma} = 0.1$ is the standard deviation of the distribution. The mobility of sodium in the Stern layer is assumed to be equal to its value in the bulk pore water. The cementation exponent is taken equal to 2. A comparison between the model and the experimental data is shown in Figure 14. We find an excellent agreement between the model and the data.

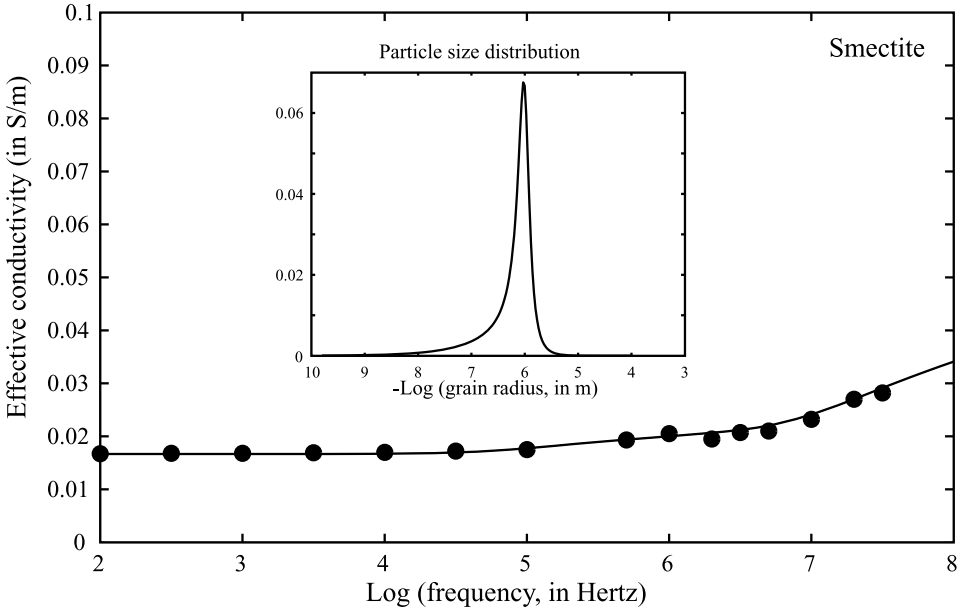


Figure 16. Comparison between the experimental data of *Arulanandan* [1969] and the prediction of the differential effective medium approach for a Na-montmorillonite (smectite). The PSD being unknown, we use a Cole-Cole distribution for the PSD (see the insert and Table 8).

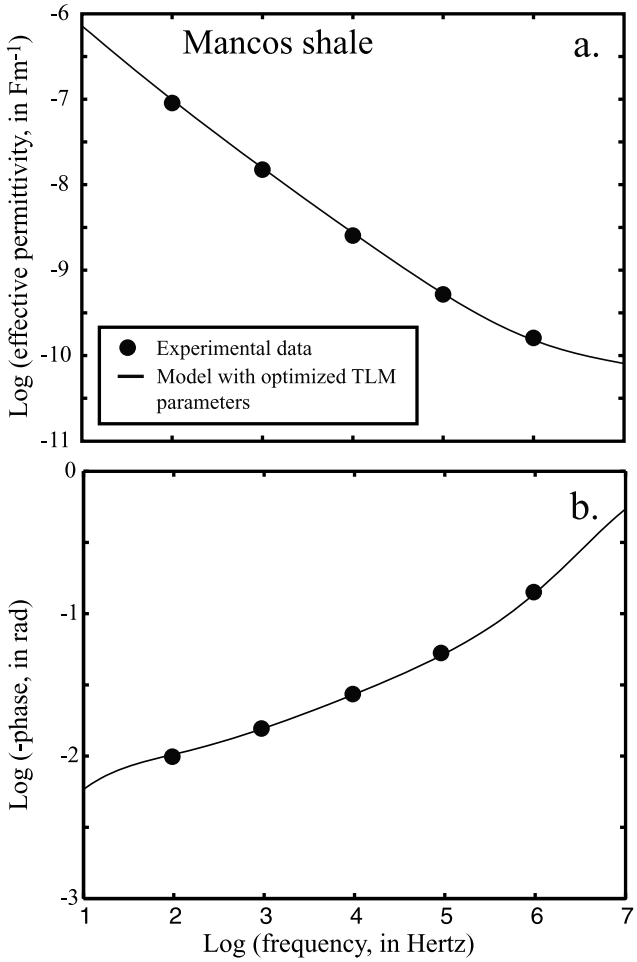


Figure 17. Comparison between the experimental data of *Scott et al.* [1967] and the prediction of the volume averaging approach (see parameters in Table 9). (a) Effective dielectric constant. (b) Phase angle (see equation (30)).

[42] For illite, we consider that the elementary particles have a diameter of 50 nm and a thickness of 6 nm [*Hassan et al.*, 2006]. The different particles form aggregates (tactoids) with a size that is much larger than the previous values. The value of the CEC used to determine the conductivity of the pore water by taking $\overline{\sigma}_f \approx \beta_{(+)}\overline{Q}_V$ is obtained from *Mehran and Arulanandan* [1977] for the Grundite illite (CEC = 0.2 meq g^{-1}). The cementation exponent is taken equal to 2.5. Note that the pore fluid conductivity calculated by the model is, in the case of illite and smectite, one order of magnitude higher than the pore fluid conductivity mentioned by *Arulanandan* [1969] (see Table 6). As explained above, this is not surprising in highly charged media like illite and smectite because of the influence of the electrical diffuse layer. Extraction obtained by squeezing the porous material cannot provide representative pore water conductivities as discussed by *Leroy et al.* [2007].

[43] For smectite, the elementary clay particle is formed by a pile of ten sheets as shown in Figure 5. To determine the conductivity of the pore water $\overline{\sigma}_f$, we use $\overline{\sigma}_f \approx \beta_{(+)}\overline{Q}_V$. The effective CEC required to determine $\overline{Q}_V$ is equal to the CEC of an elementary layer (1 meq g^{-1}) divided by the number of layers per particle. This yields an effective CEC of 0.1 meq g^{-1}. The cementation exponent is taken equal to 3.

[44] The best fits between the SIP model and the experimental data are shown in Figure 14 for the kaolinite samples, in Figure 15 for the illlite sample, and in Figure 16 for the smectite sample. The optimized parameters (Γ^0_{Na} and Γ^d_{Na}) are reported in Tables 7 and 8. For all the minerals, we found an excellent agreement between the values of the surface concentrations in the Stern and diffuse layers resulting from the TLM calculations and those determined from the experimental data (compare the optimized values of Γ^0_{Na} and Γ^d_{Na} in Tables 7 and 8 from SIP data to the TLM-derived values reported in Table 5).

4.3. Clay Rocks

[45] To test our model for clay rocks, we use the effective conductivity and permittivity data of *Scott et al.* [1967] who used the Mancos shale. The Mancos shale is an early Cretaceous dark gray carbonaceous clay rock from eastern Utah with illite (pure illite and smectite/illite mixed layer clays) [*Nadeau and Reynolds*, 1981]. The clay fraction φ_c is roughly equal to 0.45 [*Nadeau and Reynolds*, 1981] while the other minerals are carbonates and silica. The pH of the solution is considered equal to 8 because of the presence of the carbonates. The CEC of the clay fraction is equal to 0.3 meq g^{-1} [*Jaynes and Bigham*, 1986]. The porosity of the clay fraction is 0.07. Consequently, using equation (51), the total porosity of the Mancos shale is 0.03. The salinity of the water in contact with the material is assumed to be equal to 10^{-3} mol L^{-1} (distilled water plus the effect of carbonate dissolution). To determine the conductivity of the pore water of the clay rock, we use the low-salinity asymptotic limit $\overline{\sigma}_f \approx \beta_{(+)}\overline{Q}_V$ discussed in section 3 because *Scott et al.* [1967] used distilled water for their experiments.

[46] We use $\beta_{Na} = 5.19 \times 10^{-8}$ $m^2 s^{-1} V^{-1}$, $\beta_{Cl} = 8.47 \times 10^{-8}$ $m^2 s^{-1} V^{-1}$ in the pore water and $\beta^S_{Na} = 5.19 \times$

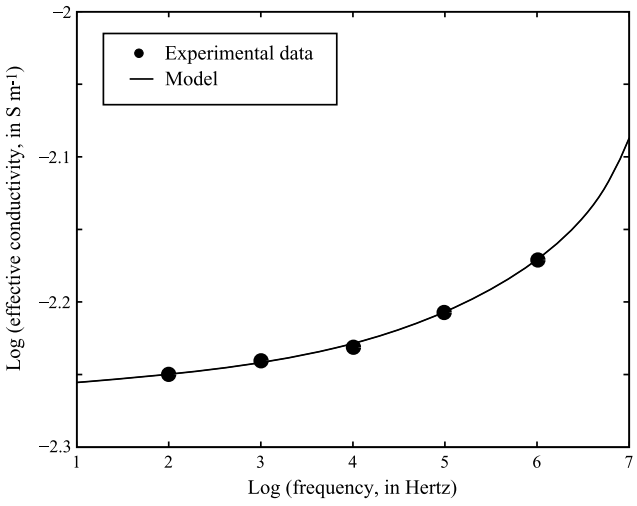


Figure 18. Comparison between the experimental data of *Scott et al.* [1967] and the prediction of the model based on the volume averaging approach concerning the effective conductivity (in S m^{-1}) (see parameters in Table 9).

Table 9. Values of the Material Properties Needed to Model the SIP Experiments Made by *Scott et al.* [1967] With the Mancos Shale[a]

Parameter	Mancos Shale
m	2.2
ϕ	0.03
ϕ_c[b]	0.07
Γ^0_{Na} (nm^{-2})	1.12 ± 0.2
Γ^d_{Na} (nm^{-2})	0.2 ± 0.1
f_Q[c]	0.85
d (μm)	4 ± 2
c[d]	0.76 ± 0.05
β^S_{Na} ($m^2\ s^{-1}\ V^{-1}$)	0.52×10^{-8}

[a]NaCl, pH ∼8.
[b]Porosity of the clay fraction.
[c]Determined from $f_Q = \Gamma^0_{Na}/(\Gamma^0_{Na} + \Gamma^d_{Na})$.
[d]Cole-Cole exponent.

10^{-9} $m^2s^{-1}V^{-1}$ in the Stern layer [see *Revil et al.*, 1998]. The size of the tactoids is 4 μm. Comparisons between the SIP model and the experimental data are shown in Figures 17 and 18. The optimized values of Γ^0_{Na} and Γ^d_{Na} are reported in Table 9. The surface densities Γ^0_{Na} and Γ^d_{Na} are in very good agreement with the TLM calculations reported in Table 5 (illite, salinity of 10^{-3} mol L^{-1}).

4.4. TLM and SIP-Derived Surface Sites Densities

[47] In Figure 19, we plot the surface site densities of the counterions in the Stern layer and in the diffuse layer optimized to reproduce the SIP data as a function of the values of these parameters as determined from the TLM described in section 2. The excellent agreement between both sets of values is remarkable and indicates that the polarization of the electrical triple layer is of paramount importance to explain SIP data. The strength of the present model is coming from the fact that it is able to explain many other transport properties of clay-rich materials [see, e.g., *Jougnot et al.*, 2009]. This provides a unified framework in which parameters derived from the measurement of some properties (like SIP) can be used to infer other transport properties (like permeability or the diffusivity of ions in the porous material for instance).

5. Discussion

[48] In our modeling approach, we have assumed that the diffuse layer does not polarize and we have neglected the potential contribution associated with the so-called constrictivity effect of the pores [see *Marshall and Madden*, 1959; *Titov et al.*, 2002]. This contribution is also called the membrane polarization (M-P) contribution in the literature. Because we were able to model the SIP spectra in the frequency range 1 Hz to 1 Mz without the need for flush factors, it seems that our assumption regarding the fact the M-P contribution can be neglected in the frequency range 1 Hz to 1 MHz is correct. What about very low frequencies, below 1 Hz? Figure 20 shows the SIP spectrum for a bentonite (data from *Olhoeft* [1985]). While we can easily recognize the Maxwell-Wagner polarization (MW-P) and the polarization of the Stern layer (S-P) coating the silt grains, there is clearly a third polarization mechanism existing at very low frequencies (1 mHz to 1 Hz). The total

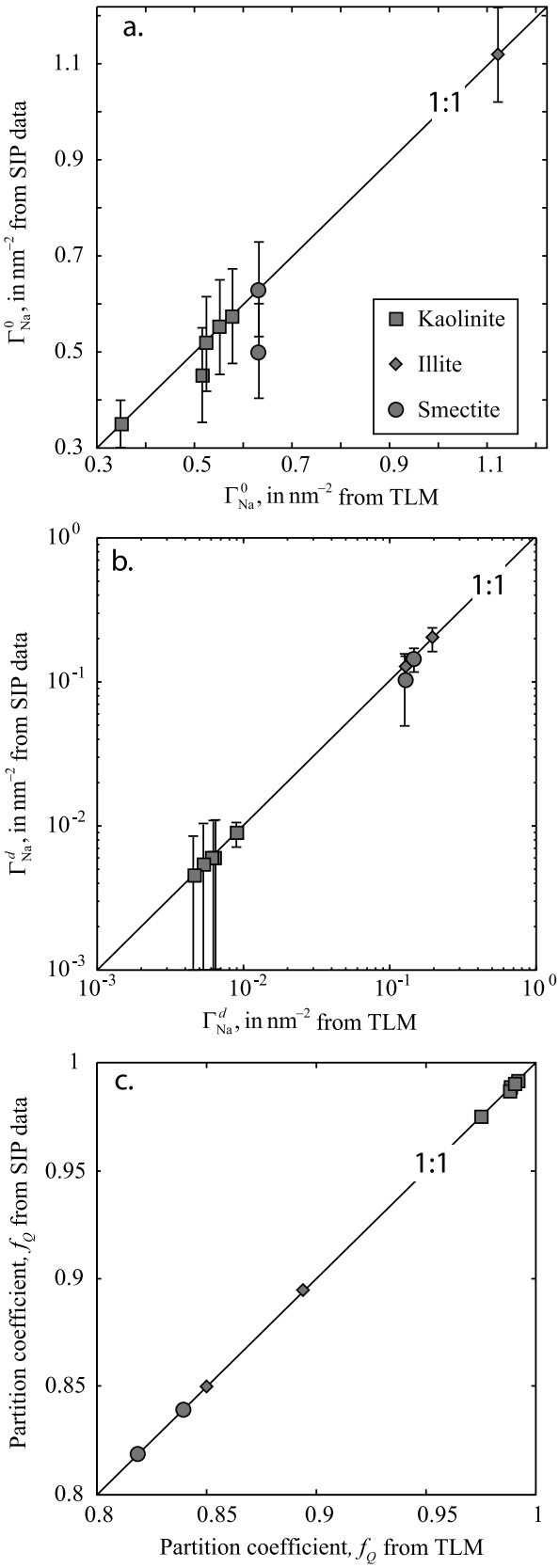


Figure 19. Comparison between the surface site densities (a) in the Stern layer and (b) in the diffuse layer determined from the spectral induced polarization data and those determined from the triple layer model. (c) Comparison for the partition coefficient.

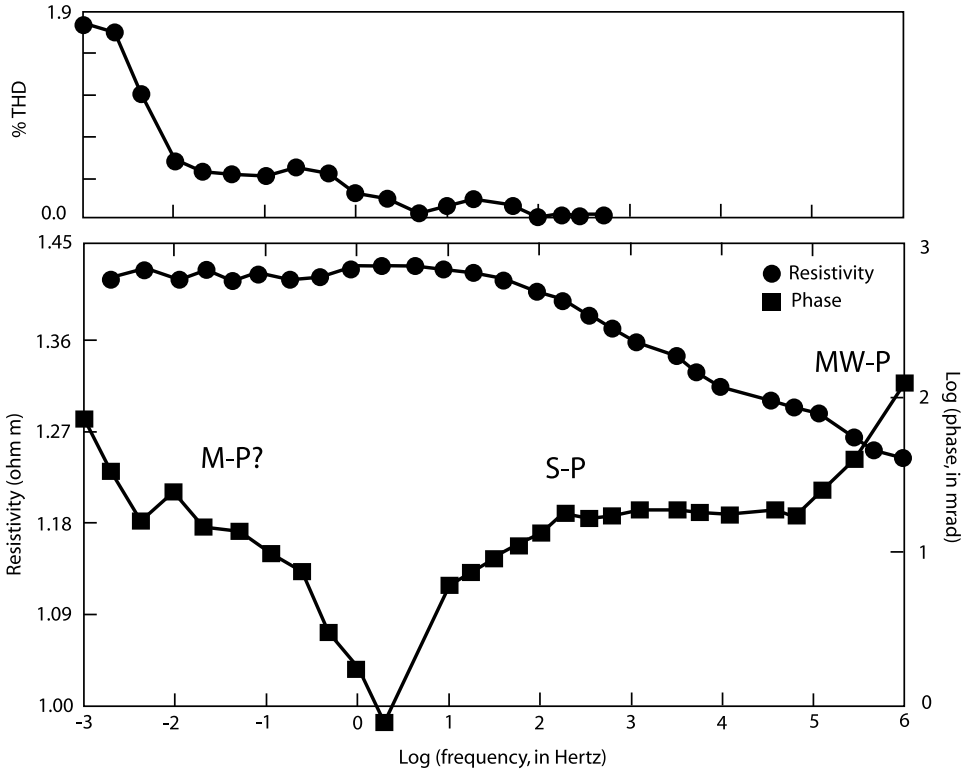


Figure 20. The complex resistivity spectrum of American Petroleum Institute standard bentonite API-26 from Clay Spur, Wyoming, composed of three parts 0.1 mol L^{-1} KCl solution to two parts dry clay by weight (experimental data from *Olhoeft* [1985]). The spectrum is the superposition of three contributions: at high frequencies (>10^5 Hz), the response is dominated by the Maxwell-Wagner polarization (MW-P). At intermediate frequencies (1 to 10^5 Hz), the main contribution results from the polarization of the Stern layer of the silt grains. At low frequencies (<1 Hz), the membrane polarization could represent the main contribution to the polarization of the material. This nonlinear polarization process would be consistent with the THD spectrum shown by the data at low frequencies.

harmonic distortion (THD) represents the root-mean-square difference between the deconvoluted harmonic content of current stimulus and voltage response. High THD can represent the signature of a nonlinear charge storage mechanism [*Olhoeft*, 1985]. Because membrane polarization is a nonlinear polarization mechanism by essence [*Marshall and Madden*, 1959], it is tempting to associate the low-frequency polarization observed by *Olhoeft* [1985] (Figure 20) to this mechanism. We plan to devote a future work on modeling this contribution for clays.

6. Conclusions

[49] We investigated the low-frequency electrical properties of clay-rich media in various states of compaction, including clay gels, compacted clay media, and clay rocks. Our model is able to represent the conductivity and permittivity spectra of these media, at least for simple supporting electrolytes. A very different behavior is found to occur between kaolinite on one side and illite and smectite on the other. Kaolinite is characterized by lateral crystalline plane reactivity ({110} and {010} planes), low CEC, low specific surface area, low value of the cementation exponent, and a porosity mainly dominated by the bulk pore water. The fraction of counterions in the Stern layer is very high ($\sim$0.98 ± 0.02) but the mobility of the counterions in the Stern layer seems to be identical to its value in the bulk pore water (a similar result was found for glass beads by *Leroy et al.* [2008] that may indicate a very weak sorption of sodium and potassium in the Stern layer of these minerals).

[50] At the opposite, the electrochemical reactivity of illite and smectite is localized on the basal {001} crystalline plane. Illite and smectite are also characterized by high cation exchange capacity, high specific surface areas, high values of the cementation exponent related to the high aspect ratio of the clay particles or the tactoids, and a strong influence of the diffuse layer upon the properties of the pore water phase. The fraction of counterions in the Stern layer is much lower than in kaolinite (typically $\sim$0.80 ± 0.05) and the mobility of sodium in the Stern layer is approximately ten times smaller than in the bulk pore water.

Appendix A

[51] Ampère law is written as

$$\nabla \times \mathbf{H} = \mathbf{J} + \frac{\partial \mathbf{D}}{\partial t}, \tag{A1}$$

where t is time (in seconds), $\mathbf{J}$ is the conduction current density (in A m^{-2}), $\mathbf{H}$ is the magnetic field (in A m^{-1}),

$\mathbf{D} = \varepsilon\,\mathbf{E}$ is the dielectric displacement (in C m^{-2}), and ε is the permittivity (in F m^{-1}) of the material ($\varepsilon/\varepsilon_0$ is the relative permittivity). The current density is given by Ohm's law, $\mathbf{J} = \sigma\,\mathbf{E}$ with the harmonic electrical field $\mathbf{E} = \mathbf{E}_0 \exp(i\omega t)$ and ω is the angular frequency. The total current density is the sum of a conduction current plus a displacement current $\mathbf{J}_t = (\sigma + i\omega\varepsilon)\mathbf{E}$, where σ and ε are complex scalars dependent upon frequency, $\sigma = \sigma' + i\sigma''$ and $\varepsilon = \varepsilon' + i\varepsilon''$. The total current density can be written as

$$\mathbf{J}_t = \sigma^*\mathbf{E}, \tag{A2}$$

where $\sigma^* = \sigma_{eff} + i\omega\varepsilon_{eff}$ is the effective or apparent conductivity and σ_{eff} and ε_{eff} are real scalars dependent upon frequency. These effective parameters are the parameters that are measured during an experiment in the laboratory or in the field. They are given by $\sigma_{eff} = \sigma' - \omega\varepsilon''$ and $\varepsilon_{eff} = \varepsilon' + \sigma''/\omega$ (note that $-\omega\varepsilon''$ is always positive). Therefore the effective conductivity includes contributions from charge conduction and polarization mechanisms. Similarly, the effective permittivity has contributions from both Ohmic and dielectric processes. The low frequency data can be displayed as the function of the frequency $f = \omega/(2\pi)$.

Appendix B

[52] Rather than using a lognormal distribution for the grain size (see equation (52)), one may prefer a Cole-Cole distribution [see *Lesmes and Morgan*, 2001]. The distribution of the relaxation time is given by [*Cole and Cole*, 1941]

$$F(\ln\tau) = \frac{1}{2\pi}\frac{\sin[\pi(1-c)]}{\cosh[c\ln(\tau/\tau_0)] - \cos[\pi(1-c)]}, \tag{B1}$$

where c is the Cole-Cole exponent This distribution is symmetric about $\tau = \tau_0$ and is similar to a Gaussian distribution when $0.5 \leq c \leq 1$. The tails are becoming increasingly broad as c decreases. This yields the following expression for the surface conductivity:

$$\sigma_s = \sigma_s^\infty + \frac{\sigma_s^0 - \sigma_s^\infty}{1 + (i\omega\tau_0)^c}, \tag{B2}$$

$$\sigma_s^0 = \frac{2}{a_0}\Sigma_S^0, \tag{B3}$$

$$\sigma_s^\infty = \frac{2}{a_0}\left(\Sigma_S^0 + \Sigma_S^\infty\right), \tag{B4}$$

In the limit $c = 1$, we recover the Debye distribution corresponding to a Dirac distribution for the particle size distribution. The distribution of relaxation times is related to the particle size distribution by the equations described by *Lesmes and Morgan* [2001].

[53] **Acknowledgments.** We thank C. Tournassat and G. Olhoeft for fruitful discussions. We thank the Associate Editor and one referee for their constructive reviews. We thank NSF for funding (grant NSF EAR-0711053).

References

Alali, F. (2007), Dependence of NMR and SIP parameters on clay content, M.Sc. thesis, Tech. Univ. Berlin, Germany.

Archie, G. E. (1942), The electrical resistivity log as an aid in determining some reservoir characteristics, *Trans. Am. Inst. Min. Metall. Pet. Eng.*, *146*, 54–61.

Arulanandan, K. (1969), Hydraulic and electrical flows in clays, *Clays Clay Miner.*, *17*, 63–76, doi:10.1346/CCMN.1969.0170204.

Avena, M. J., and C. P. De Pauli (1996), Modeling the interfacial properties of an amorphous aluminosilicate dispersed in aqueous NaCl solutions, *Colloids Surf. A*, *118*, 75–87, doi:10.1016/0927-7757(96)03668-0.

Ballario, C., A. Bonincontro, and C. Cametti (1976), Dielectric dispersions of colloidal particles in aqueous suspensions with low ionic conductivity, *J. Colloid Interface Sci.*, *54*(3), 415–423, doi:10.1016/0021-9797(76)90321-0.

Bolève, A., A. Crespy, A. Revil, F. Janod, and J. L. Mattiuzzo (2007), Streaming potentials of granular media: Influence of the Dukhin and Reynolds numbers, *J. Geophys. Res.*, *112*, B08204, doi:10.1029/2006JB004673.

Börner, F., and J. Schön (1991), A relation between the quadrature component of electrical conductivity and the specific surface area of sedimentary rocks, *Log Anal.*, *32*, 612–613.

Börner, F., M. Gruhne, and J. Schön (1993), Contamination indications derived from electrical properties in the low frequency range, *Geophys. Prospect.*, *41*, 83–98, doi:10.1111/j.1365-2478.1993.tb00566.x.

Bruggeman, D. A. G. (1935), Berechung verschieder physikalischer konstanten von heterogenen substranzen, *Ann. Phys.*, *24*, 639–679.

Cole, K. S., and R. H. Cole (1941), Dispersion and absorption in dielectrics. I. Alternating current characteristics, *J. Chem. Phys.*, *9*, 341–351, doi:10.1063/1.1750906.

Cosenza, P., A. Ghorbani, A. Revil, M. Zamora, M. Schmutz, D. Jougnot, and N. Florsch (2008), A physical model of the low-frequency electrical polarization of clay-rocks, *J. Geophys. Res.*, *113*, B08204, doi:10.1029/2007JB005539.

Crespy, A., A. Bolève, and A. Revil (2007), Influence of the Dukhin and Reynolds numbers on the apparent zeta potential of granular media, *J. Colloid Interface Sci.*, *305*, 188–194, doi:10.1016/j.jcis.2006.09.038.

Davidson, D. W., and R. H. Cole (1951), Dielectric relaxation in glycerol, propylene glycol, and *n*-propanol, *J. Chem. Phys.*, *19*(12), 1484–1490, doi:10.1063/1.1748105.

De Lima, O. A. L., and M. M. Sharma (1992), A generalized Maxwell-Wagner theory for membrane polarization in shaly sands, *Geophysics*, *57*(3), 431–440, doi:10.1190/1.1443257.

Dukhin, S. S., and V. N. Shilov (1974), *Dielectric Phenomena and the Double Layer in Disperse Systems and Polyelectrolytes*, John Wiley, New York.

Endres, A. L., and R. J. Knight (1992), A model for incorporating surface phenomena into effective medium theories for the dielectric properties of porous rocks, *Eos Trans. AGU*, *73*(43), Fall Meet. Suppl., F499.

Fixman, M. (1980), Charged macromolecules in external fields. I. The sphere, *J. Phys. Chem.*, *72*, 5177–5186, doi:10.1063/1.439753.

Ghorbani, A., C. Camerlynck, N. Florsch, P. Cosenza, A. Tabbagh, and A. Revil (2007), Bayesian inference of the Cole-Cole parameters from time and frequency-domain induced polarization, *Geophys. Prospect.*, *55*(4), 589–605, doi:10.1111/j.1365-2478.2007.00627.x.

Gonçalvès, J., P. Rousseau-Gueutin, and A. Revil (2007), Introducing interacting diffuse layers in TLM calculations: A reappraisal of the influence of the pore size on the swelling pressure and the osmotic efficiency of compacted bentonites, *J. Colloid Interface Sci.*, *316*(1), 92–99, doi:10.1016/j.jcis.2007.07.023.

Grimm, R. E., R. Olhoeft, K. McKinley, J. Rossabi, and B. Riha (2005), Nonlinear complex resistivity survey for DNAPL at the Savannah river site A-014 outfall, *J. Environ. Eng. Geophys.*, *10*(4), 351–364.

Hanai, T. (1968), Electrical properties of emulsions, in *Emulsions Science*, edited by P. Sherman, pp. 354–477, Academic, San Diego, Calif.

Hassan, M. S., F. Villieras, F. Gaboriaud, and A. Razafitianamaharavo (2006), AFM and low-pressure argon adsorption analysis of geometrical properties of phyllosilicates, *J. Colloid Interface Sci.*, *296*(2), 614–623, doi:10.1016/j.jcis.2005.09.028.

Hördt, A., R. Blaschek, A. Kemna, and N. Zisser (2007), Hydraulic conductivity estimation from induced polarization data at the field scale–The Krauthausen case history, *J. Appl. Geophys.*, *62*(1), 33–46, doi:10.1016/j.jappgeo.2006.08.001.

Hunter, R. J. (1981), *Zeta Potential in Colloid Science: Principles and Applications*, Academic, San Diego, Calif.

Jaynes, W. F., and J. M. Bigham (1986), Multiple cation-exchange capacity measurements on standard clays using a commercial mechanical extractor, *Clays Clay Miner.*, *34*(1), 93–98, doi:10.1346/CCMN.1986.0340112.

Jonscher, A. K. (1983), *Dielectric Relaxation in Solids*, Chelsea Dielectric, London.

Jougnot, D., A. Revil, and P. Leroy (2009), Diffusion of ionic tracers in the Callovo-Oxfordian clay-rock using the Donnan equilibrium model and the electrical formation factor, *Geochim. Cosmochim. Acta*, *73*(10), 2712–2726, doi:10.1016/j.gca.2009.01.035.

Kemna, A., A. Binley, and L. Slater (2004), Crosshole IP imaging for engineering and environmental applications, *Geophysics*, *69*(1), 97–107, doi:10.1190/1.1649379.

Korosak, D., B. Cvikl, J. Kramer, R. Jecl, and A. Prapotnik (2007), Fractional calculus applied to the analysis of spectral electrical conductivity of clay-water system, *J. Contam. Hydrol.*, *92*(1–2), 1–9, doi:10.1016/j.jconhyd.2006.11.005.

Leroy, P., and A. Revil (2004), A triple-layer model of the surface electrochemical properties of clay minerals, *J. Colloid Interface Sci.*, *270*(2), 371–380, doi:10.1016/j.jcis.2003.08.007.

Leroy, P., A. Revil, and D. Coelho (2006), Diffusion of ionic species in bentonite, *J. Colloid Interface Sci.*, *296*(1), 248–255, doi:10.1016/j.jcis.2005.08.034.

Leroy, P., A. Revil, S. Altmann, and C. Tournassat (2007), Modeling the composition of the pore water in a clay-rock geological formation (Callovo-Oxfordian, France), *Geochim. Cosmochim. Acta*, *71*(5), 1087–1097, doi:10.1016/j.gca.2006.11.009.

Leroy, P., A. Revil, A. Kemna, P. Cosenza, and A. Gorbani (2008), Spectral induced polarization of water-saturated packs of glass beads, *J. Colloid Interface Sci.*, *321*(1), 103–117, doi:10.1016/j.jcis.2007.12.031.

Lesmes, D. P., and F. D. Morgan (2001), Dielectric spectroscopy of sedimentary rocks, *J. Geophys. Res.*, *106*(B7), 13,329–13,346, doi:10.1029/2000JB900402.

Lockhart, N. C. (1980a), Electrical properties and the surface characteristics and structure of clays, *I. Swelling clays, J. Colloid Interface Sci.*, *74*(2), 509–519, doi:10.1016/0021-9797(80)90220-9.

Lockhart, N. C. (1980b), Electrical properties and the surface characteristics and structure of clays. II. Kaolinite—A nonswelling clay, *J. Colloid Interface Sci.*, *74*(2), 520–529, doi:10.1016/0021-9797(80)90221-0.

Lyklema, J., S. S. Dukhin, and V. N. Shilov (1983), The relaxation of the double layer around colloidal particles and the low-frequency dielectric dispersion. Part 1. Theoretical considerations, *J. Electroanal. Chem.*, *143*, 1–21, doi:10.1016/S0022-0728(83)80251-4.

Mansoor, N., and L. Slater (2007), On the relation between iron concentration and induced polarization in marsh soil, *Geophysics*, *72*(1), A1–A5, doi:10.1190/1.2374853.

Marshall, D. J, and T. R. Madden (1959), Induced polarization: A study of its cause, *Geophysics*, *24*, 790–816, doi:10.1190/1.1438659.

Maxwell, J. C. (1892), *A Treatise on Electricity and Magnetism*, 3rd ed., Oxford Univ. Press, London.

Mehran, P. H., and K. Arulanandan (1977), Low frequency conductivity dispersion in clay-water-electrolyte systems, *Clays Clay Miner.*, *25*(1), 39–48, doi:10.1346/CCMN.1977.0250107.

Mendelson, K. S., and M. H. Cohen (1982), The effect of grain anisotropy on the electrical-properties of sedimentary rocks, *Geophysics*, *47*(2), 257–263, doi:10.1190/1.1441332.

Nadeau, P. H., and R. C. Reynolds (1981), Burial and contact metamorphism in the Mancos shale, *Clays Clay Miner.*, *29*(4), 249–259, doi:10.1346/CCMN.1981.0290402.

Olhoeft, G. R. (1979), Electrical properties, in *Initial Report of the Petrophysics Laboratory*, edited by H. G. Hunt et al., *U. S. Geol. Surv. Circ.*, *789*, 1–25.

Olhoeft, G. R. (1985), Low-frequency electrical properties, *Geophysics*, *50*, 2492–2503, doi:10.1190/1.1441880.

Park, S. K., and S. K. Dickey (1989), Accurate estimation of conductivity of water from geoelectrical measurements—A new way to correct for clay, *Ground Water*, *27*(6), 786–792, doi:10.1111/j.1745-6584.1989.tb01042.x.

Poley, J. P., J. J. Nooteboom, and P. J. de Waal (1978), Use of V. H. F. dielectric measurements for borehole formation analysis, *Log Anal.*, *19*, 8–30.

Radic, T. (2007), Multi-source SIP, paper presented at Treffen des Arbeitskreis Induzierte Polarisation der Deutschen Geophysikalischen Gesellschafte V, Bundesanst. für Materialforsch. und -prüfung, Berlin, Germany.

Revil, A. (2000), Thermal conductivity of unconsolidated sediments with geophysical applications, *J. Geophys. Res.*, *105*(B7), 16,749–16,768, doi:10.1029/2000JB900043.

Revil, A., and P. W. J. Glover (1997), Theory of ionic surface electrical conduction in porous media, *Phys. Rev. B*, *55*(3), 1757–1773, doi:10.1103/PhysRevB.55.1757.

Revil, A., and P. Leroy (2001), Hydroelectric coupling in a clayey material, *Geophys. Res. Lett.*, *28*(8), 1643–1646, doi:10.1029/2000GL012268.

Revil, A., and P. Leroy (2004), Constitutive equations for ionic transport in porous shales, *J. Geophys. Res.*, *109*, B03208, doi:10.1029/2003JB002755.

Revil, A., and N. Linde (2006), Chemico-electromechanical coupling in microporous media, *J. Colloid Interface Sci.*, *302*(2), 682–694, doi:10.1016/j.jcis.2006.06.051.

Revil, A., L. M. Cathles, S. Losh, and J. A. Nunn (1998), Electrical conductivity in shaly sands with geophysical applications, *J. Geophys. Res.*, *103*(B10), 23,925–23,936, doi:10.1029/98JB02125.

Samec, M., D. Korosak, and B. Cviki (2007), Probing ion in a clay-water system with dielectric spectroscopy, *Acta Geotech. Slovenica*, *4*(1), 4–9.

Santiwong, S. R., J. Guan, and T. D. Waite (2008), Effect of the ionic strength and pH on the hydraulic properties of accumulating solid assemblages during microfiltration of montmorillonite suspensions, *J. Colloid Interface Sci.*, *317*(1), 214–227, doi:10.1016/j.jcis.2007.09.052.

Schurr, J. M. (1964), On the theory of the dielectric dispersion of spherical colloidal particles in electrolyte solution, *J. Phys. Chem.*, *68*, 2407–2413, doi:10.1021/j100791a004.

Schwan, H. P., G. Schwarz, J. Maczuk, and H. Pauly (1962), On the low-frequency dielectric dispersion of colloidal particles in electrolyte solution, *J. Phys. Chem.*, *66*, 2626–2635, doi:10.1021/j100818a066.

Schwarz, G. (1962), A theory of the low-frequency dielectric dispersion of colloidal particles in electrolyte solution, *J. Phys. Chem.*, *66*, 2636–2642, doi:10.1021/j100818a067.

Scott, J. B. T., and R. D. Barker (2003), Determining pore-throat size in Permo-Triassic sandstones from low-frequency electrical spectroscopy, *Geophys. Res. Lett.*, *30*(9), 1450, doi:10.1029/2003GL016951.

Scott, J. H., R. D. Caroll, and D. R. Cunningham (1967), Dielectric constant and electrical conductivity measurements of moist rock: A new laboratory method, *J. Geophys. Res.*, *72*, 5101–5115, doi:10.1029/JZ072i020p05101.

Sen, P. N., C. Scala, and M. H. Cohen (1981), A self-similar model for sedimentary rocks with application to the dielectric constant of fused glass beads, *Geophysics*, *46*(5), 781–795, doi:10.1190/1.1441215.

Slater, L. (2007), Near surface electrical characterization of hydraulic conductivity. From petrophysical properties to aquifer geometries. A review, *Surv. Geophys.*, *28*, 169–197, doi:10.1007/s10712-007-9022-y.

Slater, L., and D. Lesmes (2002), IP interpretation in environmental investigations, *Geophysics*, *67*(1), 77–88, doi:10.1190/1.1451353.

Sogade, J. A., F. Scira-Scappuzzo, Y. Vichabian, W. Shi, W. Rodi, D. P. Lesmes, and F. D. Morgan (2006), Induced-polarization detection and mapping of contaminant plumes, *Geophysics*, *71*(3), B75–B84, doi:10.1190/1.2196873.

Tarasov, A., and K. Titov (2007), Relaxation time distribution from time domain polarization measurements, *Geophys. J. Int.*, *170*(1), 31–43, doi:10.1111/j.1365-246X.2007.03376.x.

Titov, K., V. Komarov, V. Tarasov, and A. Levitski (2002), Theoretical and experimental study of time-domain induced polarization in water-saturated sands, *J. Appl. Geophys.*, *50*, 417–433, doi:10.1016/S0926-9851(02)00168-4.

Tournassat, C., A. Neaman, F. Villiéras, and L. Charlet (2003), Nanomorphology of Montmorillonite particles: Estimation of the clay edge sorption site density by low-pressure gas adsorption and AFM observations, *Am. Mineral.*, *88*, 1989–1995.

Tournassat, C., E. Ferrage, C. Poinsignon, and L. Charlet (2004), The titration of clay minerals. Part II. Structural-based model and implications for clay reactivity, *J. Colloid Interface Sci.*, *273*(1), 234–246, doi:10.1016/j.jcis.2003.11.022.

Vinegar, H. J., and M. H. Waxman (1982), Method and apparatus for determining shaliness and oil saturations in earth formations using induced polarization in the frequency domain, Patent 4,359,687, U. S. Patent and Trademark Off, Washington, D. C.

Vinegar, H. J., and M. H. Waxman (1984), Induced polarization of shaly sands, *Geophysics*, *49*, 1267–1287, doi:10.1190/1.1441755.

Vinegar, H. J., and M. H. Waxman (1987), In-situ method for determining pore size distribution, capillary pressure and permeability, Patent 4,644,283, U. S. Patent and Trademark Off, Washington, D. C.

Wagner, K. W. (1914), Erklarung des dielektrischen Nachwirkungen auf Grund Maxwellisher Vortellungen, *Arch. Electr.*, *2*, 371–387, doi:10.1007/BF01657322.

Wait, J. R. (1984), Relaxation time phenomena and induced polarization, *Geoexploration*, *22*, 107–127, doi:10.1016/0016-7142(84)90032-2.

Weller, A., and F. D. Börner (1996), Measurements of spectral induced polarization for environmental purposes, *Environ. Geophys.*, *27*, 329–334.

Zhdanov, M. S., and G. V. Keller (1994), *The Geoelectrical Methods in Geophysical Exploration*, 873 pp., Elsevier, Amsterdam.

P. Leroy, BRGM, 3 avenue Claude Guillemin, F-45060 Orléans, France.
A. Revil, Department of Geophysics, Colorado School of Mines, 1500 Illinois Street, Golden, CO 80401, USA. (arevil@mines.edu)